NASA-TM-75877 19810010501

NASA TECHNICAL MEMORANDUM

NASA TM-75877

SEPARATION BEHAVIOR OF BOUNDARY LAYERS ON THREE-DIMENSIONAL WINGS

H. W. Stock

Translation of "Ablöseverhalten von Grenzschichten an dreidimensionalen Flügeln", Dornier GmbH, Friedrichshafen, West Germany, No. T/RF 41/800052 / 81451, October 1979, 86 pages.

NATIONAL AERONAUTICS AND SPACE ADMINISTRATION
WASHINGTON, D.C. 20546 FEBRUARY 1981

STANDARD TITLE PAGE

1. Report No. NASA TM-75877	2. Government Accession No.	3. Recipient's Catalog No.
4. Title and Subtitle: SEPARATION BEHAVIOR OF BOUNDARY LAYERS ON THREE-DIMENSIONAL WINGS		5. Report Date February 1981 6. Performing Organization Code
7. Author(s) H.W. Stock, Dornier GmbH		8. Performing Organization Report No. 10. Work Unit No.
9. Performing Organization Name and Address Leo Kanner Associates, Redwood City, California 94063		11. Contract or Grant No. NASw-3199 13. Type of Report and Period Covered Translation
12. Sponsoring Agency Name and Address National Aeronautics and Space Administration, Washington, D.C. 20546		14. Sponsoring Agency Code

15. Supplementary Notes

Translation of "Ablöseverhalten von Grenzschichten an dreidimensionalen Flügeln", Dornier GmbH, Friedrichshafen, West Germany, No. T/RF 41/800052 / 81451, October 1979, 86 pages.

16. Abstract

An inverse boundary layer procedure for calculating separated, turbulent boundary layers at infinitely long, crabbing wings has been developed. The procedure developed at Dornier for calculating three-dimensional, incompressible turbulent boundary layers has been expanded to adiabatic, compressible flows. Example calculations with transsonic wings have been made, including viscose effects. In this case an approximated calculation method has been described for areas of separated, turbulent boundary layers, permitting calculation of the displacement thickness. The laminar boundary layer development has been calculated with inclined ellipsoids.

17. Key Words (Selected by Author(s))	18. Distribution Statement: Unclassified-Unlimited		
19. Security Classif. (of this report) Unclassified	20. Security Classif. (of this page) Unclassified	21. No. of Pages	22. Price

NASA-HQ

SEPARATION BEHAVIOR OF BOUNDARY LAYERS ON THREE-DIMENSIONAL WINGS

H. W. Stock

Dornier GmbH

Table of Contents

Survey /1*

Four working points are treated in this report.

1. An inverse integral procedure for calculating separated, turbulent boundary layers at infinitely long, crabbing wings is described. The concept of calculating inversely into the separation area with the boundary layer equations has been extended to flows at infinitely long, crabbing wings for the first time here.

   The displacement thickness distribution of the velocity profile in the direction of wing depth is utilized as input, and the corresponding velocity at the outside edge of the boundary layer calculated according to size and direction. It is assumed that the velocity profile in the direction of main flow can be represented by the expanded Coles profile and the velocity profile in the direction of wingspan by Coles profile for the case of pressure gradient of zero.

   A comparison with measurements in a separating, turbulent boundary layer is demonstrated.

2. An integral procedure developed at Dornier for calculating three-dimensional, turbulent, incompressible boundary layers has been expanded for the adiabatic case to compressible flows.

   The integral quantities are converted by the Stewartson-Illingworth transformation and the calculation carried out in a transformed space. As a conclusion of the calculation, the calculated quantities are calculated back to the physical space. Comparisons with measurements and other procedures are shown.

3. Calculations results with three-dimensional, transsonic wings are shown, taking friction into consideration. The pressure distribution is determined iteratively with a potential and theoretical (small perturbation) procedure and a three-dimensional boundary layer procedure.

   For the case of a turbulent separation of the boundary layer in a wing section, an approximation procedure is described for calculating the separated, turbulent boundary layer.

4. The laminar boundary layer is calculated with the Dornier integral procedure with tipped rotation ellipsoids and compared with results of different procedures and measurements (DFVLR). The three-dimensional displacement surface and the lines of turbulent departure are shown.

---

*Numbers in the margin indicate pagination in the foreign text.

1. Inverse Integral Procedure for Calculating Separated, Turbulent Boundary Layers with an Infinitely Long, Crabbing Wing /3

Symbols

c_{fx}	Component of the coefficient of friction in the x direction
c_{fs}	Component of the coefficient of friction in the s direction
c_{fy}	Component of the coefficient of friction in the y direction
F	Entrainment coefficient
F_{Eq}	Entrainment coefficient in balanced boundary layers
$H_s = \delta_1^*/\theta_{11}$	Form parameter of the velocity profile in the s direction
$H_x = \delta_x^*/\theta_x$	Form parameter of the velocity profile in the x direction
$H_y = \delta_y^*/\theta_y$	Form parameter of the velocity profile in the y direction
$H_1 = \frac{\delta-\delta_1^*}{\theta_{11}}$	Form parameter of the velocity profile in the s direction
$\bar{H}_1 = \frac{\bar{\delta}-\bar{\delta}_1^*}{\bar{\theta}_{11}}$	Form parameter of the outside layer of the velocity profile in the s direction for which $U \geq 0$.
k	von Kámán constant
n	Direction of transverse flow
P_1, P_2, P_3	Quantities defined in Appendix C
s	Direction of main flow
u	Component of velocity in the x direction
U	Component of velocity in the s direction /4
v	Component of velocity in the y direction
V	Component of velocity in the n direction
x,y,z	Coordinates
z_o	Surface distance to the point in the boundary layer for which $U \equiv 0$.

α	Angle between the s and x directions
β	Surface flow line angle, angle between the resulting surface thrust direction and the s direction
$\delta = \int_0^{\delta} dz$	Boundary layer thickness
$\bar{\delta} = \int_{zo}^{\delta} dz$	Thickness of the outer layer for which $U \geq 0$
$\delta_{\Delta_1^*}$, δ_{Π}, δ_{ω}, δ_{u}	Derivations of δ according to Δ_1^*, Π, ω and u_e, Appendix C
$\Delta_1^* = \int_0^{\delta} (\frac{ue}{U_e} - \frac{u}{U_e}) dz$	Displacement thickness of the velocity profile in the x direction
$\delta_1^* = \int_0^{\delta} (1 - \frac{U}{U_e}) dz$	Displacement thickness of the velocity profile in the s direction
$\bar{\delta}_1^* = \int_{zo}^{\delta} (1 - \frac{U}{U_E}) dz$	Displacement thickness of the outside layer of the velocity profile for which $U \geq 0$
$\delta_2^* = - \int_0^{\delta} \frac{V}{U_e} dz$	Displacement thickness of the velocity profile in the n direction
$\delta_x^* = \int_0^{\delta} (1 - \frac{u}{u_e}) dz$	Displacement thickness of the velocity profile in the x direction /5
$\delta_y^* = \int_0^{\delta} (1 - \frac{v}{v_e}) dz$	Displacement thickness of the velocity profile in the y direction
δ^*	Displacement thickness of the three-dimensional boundary layer
$\Theta_{11} = \int_0^{\delta} \frac{u}{U_e} (\frac{u_e}{U_e} - \frac{u}{U_e}) dz$	Momentum loss thickness of the velocity profile in the x direction
$\theta_{11} = \int_0^{\delta} \frac{U}{U_e} (1 - \frac{U}{U_e}) dz$	Momentum loss thickness of the velocity profile in the s direction

$\tilde{\theta}_{11} = \int_{z_o}^{\delta} \frac{U}{U_e}\left(1 - \frac{U}{U_e}\right) dz$ Momentum loss thickness of the outer layer of the velocity profile in the s direction for which $U \geq 0$

$\theta_{12} = \int_{o}^{\delta} \frac{V}{U_e}\left(1 - \frac{U}{U_e}\right) dz$ Momentum loss thickness

$\theta_{21} = \int_{o}^{\delta} \frac{UV}{U_e} dz$ Momentum loss thickness

$\theta_{22} = \int_{o}^{\delta} \frac{V^2}{U_e^2} dz$ Momentum loss thickness of the velocity profile in the n direction

$\theta_x = \int_{o}^{\delta} \frac{\rho u}{\rho_e u_e}\left(1 - \frac{u}{u_e}\right) dz$ Momentum loss thickness of the velocity profile in the x direction

$\theta_y = \int_{o}^{\delta} \frac{\rho v}{\rho_e v_e}\left(1 - \frac{v}{v_e}\right) dz$ Momentum loss thickness of the velocity profile in the y direction

θ_δ θ_Π, θ_ω, θ_u Derivations of θ according to δ, Π, ω and u_e /6

ν Dynamic viscosity

Π Coles parameter

$\sigma = \left(\frac{c_{fy}}{2}\right)^{1/2}$ Surface friction parameter in the y direction

ϕ_Π, ϕ_ω Quantities defined in Appendix C

ψ Quantities defined in Appendix C

ψ_δ, ψ_Π, ψ_ω, ψ_u Derivations of ψ according to δ, Π, ω and u_e

$\omega = \left(\frac{c_{fs}}{2}\right)^{1/2}$ Surface friction parameter in the s direction

Index

e At the outside edge of the boundary layer

1.1 Introduction

/7

In spite of the progress in computer technology and in numerical methods, numerical solutions of the Navier-Stokes equations for separated flows are still very complicated today and not required for a portion of the applications. It appears sensible, on the basis of work in the past years, to calculate flows, demonstrating separation in a limited area, with the boundary layer concept.

The solutions of the boundary layer equations in the two-dimensional case, however, become singular when given the velocity distribution at the outside edge of the boundary layer (direct problem) in the separation point, where the surface friction becomes zero [1,2]. In the case of the direct problem, it becomes impossible to integrate the boundary layer equations downstream from the point of separation.

Catherall and Mangler [3] have demonstrated numerically, that separation occurs without leading to singular solutions, when a boundary layer quantity, e.g. the displacement thickness or the surface shearing stress, is given and the corresponding external flow is calculated (inverse problem). Moreover, it is shown in [3], that the usual integration direction directed downstream can be retained downstream from the point of separation.

In recent years, several inverse procedures, integral procedures [4-9] and difference procedures [10,11,12] for two dimensional, laminar and turbulent boundary layers have been developed. In the present work, an attempt is made for the first time to apply the concept of the inverse procedure to flows with infinitely long, crabbing wings.

Of course, flows can no longer be calculated with this method, /8 in which large interactions occur between the flow free of friction and that subject to friction, and the boundary layer equations no longer have any validity.

1.2 Fundamentals

The coordinate directions x and y are shown in Figure 1 with an infinitely long, crabbing wing. In addition, the direction of the resulting velocity U_e, supplying the direction of main flow s, and the velocity components in the x direction u_e and in the y direction v_e are shown. The angle between the x direction and the resulting velocity U_e is α. The angle between the main flow direction s and the direction of the resulting surface shearing force, describing the direction of the surface flow line is β.

1.2.1 Description of the Velocity Profile Families

Profile families for the velocity are described for the direction of main flow s by the expanded, double-parameter representation of Coles [12].

$$\frac{U}{\omega U_e} = \frac{1}{k} \ln \frac{z\,|\omega|\,U_e}{\nu} + \frac{|\omega|}{\omega} \frac{\Pi}{k} \left[1 - \cos\left(\pi \frac{z}{\delta}\right)\right] + 5.1 \qquad (1)$$

where k is the von Kámán constant.

This manner of writing makes possible the representation of reverse flow velocity profiles, similar to [4,6], for separated flows, $c_{fs} < 0$.

It applies that

/9

$$c_{fs} = 2\,|\omega|\,\omega$$

At the outside edge of the boundary layer δ it results from equation 1

$$1 = \frac{\omega}{k} \left[\ln \frac{\delta\,|\omega|\,U_e}{\nu} + 2 \frac{|\omega|}{\omega} \Pi + 5.1\,k\right] \qquad (3)$$

Equations 1 and 3 combined provide the representation of the velocity profile, employed for calculating the integral quantities

$$\frac{U}{U_e} = 1 - \frac{\omega}{k} \left[\Pi \frac{|\omega|}{\omega} \left\{1 + \cos\left(\pi \frac{z}{\delta}\right)\right\} - \ln \frac{z}{\delta}\right] \qquad (4)$$

The profile families in the direction of transverse flow n, normally running to the direction of the main flow s, was not formulated by the empirical approaches of Mager [13] or Johnston [14], as they are employed in the works for calculating three-dimensional, turbulent, adjacent boundary flows [15-17].

Instead, it is assumed that the velocity profile in the y direction, in which the pressure gradient is identical to zero, can be represented by profiles at a flat plate. With knowledge of the angle α and the profile U/U_e in the direction of main flow, the profiles in the n direction V/U_e can be determined.

Corresponding to equation 4, the following formulation is possible:

$$\frac{v}{v_e} = 1 - \frac{A}{k} \left[B \left\{1 + \cos\left(\pi \frac{z}{\delta}\right)\right\} - \ln \frac{z}{\delta}\right] \qquad (5)$$

For the flat plate, A = 0.0332 and B = 0.625. A and B are constant values in each calculation point, supplying a velocity profile v/v_e, similar to the 1/7 law of exponents. /10

It applies that

$$\frac{v}{U_e} = \frac{v}{v_e} \sin\alpha = \frac{U}{U_e} \sin\alpha + \frac{V}{U_e} \cos\alpha \qquad (6)$$

Therefore it results that

$$\frac{V}{U_e} = \frac{\sin\alpha}{\cos\alpha} \left[\frac{v}{v_e} - \frac{U}{U_e}\right]$$

or

$$\frac{V}{U_e} = \frac{1}{k} \frac{\sin\alpha}{\cos\alpha} \left[\left\{1 + \cos\left(\pi \frac{z}{\delta}\right)\right\}\{\Pi \mid \omega - A\,B\} - \ln \frac{z}{\delta} \{\omega - A\}\right] \qquad (7)$$

The velocity profiles in the s direction U/U_e, equation 4 and in the n direction V/U_e, equation 7, are employed for determining the corresponding integral quantities, in the s and n direction. The integral quantities in the x and y direction, in which the boundary layer development is calculated, can then be determined over the angle α in a simple manner.

1.2.2 Fundamental Equations

For solving the problem, the following equations are employed:

x impulse integral equation

$$\frac{d\,\Theta_{11}}{dx} + \Theta_{11} \frac{1}{U_e} \frac{dU_e}{dx} + \frac{\Delta_1^*}{U_e} \frac{du_e}{dx} = \frac{c_{fx}}{2} \qquad (8)$$

In Appendix A, the integral quantities Θ_{11} and Δ_1^* are defined and the calculation of Θ_{11} and Δ_1^* is simultaneously given from integral quantities in the s,n coordinate system. The components of the surface shearing force coefficient in the x direction c_{fx} is explained in Appendix C. /11

Equation 3 leads to an implicit expression for ω

$$\frac{1}{\omega} - \frac{1}{k} \ln |\omega| = \frac{1}{k} \ln (\delta U_e) + \frac{2}{k} \frac{|\omega|}{\omega} \Pi + 5.1 \qquad (9)$$

Equation 10 differentiated according to s provides

$$\frac{d\delta}{ds} + 2\delta \frac{|\omega|}{\omega} \frac{d\Pi}{ds} + \delta \left[\frac{k}{\omega^2} + \frac{1}{|\omega|}\right] \frac{d|\omega|}{ds} = - \frac{\delta}{U_e} \frac{dU_e}{ds} \qquad (10)$$

For a random quantity Q, $dQ/dy \equiv 0$ (infinitely long, crabbing wing)

$$\frac{dQ}{ds} = \frac{u_e}{U_e} \frac{dQ}{dx}, \qquad (11)$$

The surface friction equation results from this for equation 9

$$\frac{d\delta}{dx} + 2\delta \frac{|\omega|}{\omega} \frac{d\Pi}{dx} + \delta \left[\frac{k}{\omega^2} + \frac{1}{|\omega|}\right] \frac{d|\omega|}{dx} = - \frac{\delta}{U_e} \frac{dU_e}{dx} \qquad (12)$$

Since entrainment occurs in the outer area of the boundary layer and the transverse flow velocities are small there, the two-dimensional manner of consideration can be extended to the flow at infinitely long, crabbing wings, similar to the integral procedure [15-17]. The entrainment is coupled in this case to the velocity profile in the direction of main flow.

The entrainment equation is expressed as: /12

$$\frac{d}{dx}\left(\frac{u_e}{U_e}\delta - \Delta_1^*\right) + \frac{1}{U_e}\frac{dU_e}{dx}\left(\frac{u_e}{U_e}\delta - \Delta_1^*\right) = F \qquad (13)$$

The lag-entrainment concept of Horton [18] is employed for calculating the entrainment coefficient F in equation 13, taking into consideration the so-called upstream history effects on the coefficient F in a non-balanced boundary layer.

$$\frac{dF}{ds} = \frac{0.1}{\delta}\left(F_{Eq} - F\right) \qquad (14)$$

with

$$F_{Eq} = 0.122\left(\bar{H}_1 - 2.3\right)^{-1.38} \qquad (15)$$

where

$$\bar{H}_1 = \frac{\bar{\delta} - \bar{\delta}_1^*}{\bar{\theta}_{11}} \qquad (16)$$

In the case of adjacent flows

$$\bar{\delta} = \delta,\ \overline{\delta_1^*} = \delta_1^*,\ \bar{\theta}_{11} = \theta_{11} \text{ und } \bar{H}_1 = H_1.$$

In the case of a separated flow in the direction of main flow, the entrainment is related to integral quantities in a similar manner to [4], formed from the velocity profile situated above the U = 0 line. For separated flows, the calculation of the U = 0 line and the corresponding values δ_1 and δ_1^* and θ_{11} is given in Appendix B.

With equation 11, it follows for equation 13 /13

$$\frac{dF}{dx} = \frac{U_e}{u_e}\frac{0.1}{\delta}\left(F_{Eq} - F\right) \qquad (17)$$

An approach similar to that for c_{fs} in equation 10 is utilized for calculating the surface shearing force component c_{fy}.

With $c_{fy} = 2\,\sigma^2$ it follows that

$$\frac{d\sigma}{dx} = -0.03243\,\frac{1}{\delta}\,\frac{d\delta}{dx} \qquad (18)$$

Equation 18 states that the deviation in σ, i.e. c_{fy}, is coupled to the variation of δ. A prerequisite in this case is that the boundary layer thicknesses of the velocity layer profiles are identical in the s, n, x and y directions.

1.2.3 Solution of the Resulting Equation System

Five equations are available for the dependent variables Π, ω, u_e, σ and F

x momentum equation

$$\Theta_\Pi\,\frac{d\Pi}{dx} + \Theta_\omega\,\frac{d\omega}{dx} + P_1\,\frac{du_e}{dx} = \frac{cf}{2} - \Theta_\delta\,\delta_{\delta^*_x}\,\frac{d\,\delta^*_x}{dx} \qquad (21)$$

entrainment equation

$$\psi_\Pi\,\frac{d\Pi}{dx} + \psi_\omega\,\frac{d\omega}{dx} + P_2\,\frac{du_e}{dx} = F - \psi_\delta\,\delta_{\delta^*_x}\,\frac{d\delta^*_x}{dx} \qquad (22)$$

lag-entrainment equation /14

$$\frac{dF}{dx} = \frac{u_e}{u_e}\,\frac{0.1}{\delta}\,(F_{Eq} - F) \qquad (23)$$

surface friction equation in the s direction

$$\phi_{\Pi} \frac{d\Pi}{dx} + \phi_{\omega} \frac{d\omega}{dx} + P_3 \frac{du_e}{dx} = - \delta_{\delta_x^*} \frac{d\,\delta_x^*}{dx} \qquad (24)$$

surface friction equation in the y direction

$$\frac{d\sigma}{dx} = -0.03243 \frac{1}{\delta} \frac{d\delta}{dx} \qquad (25)$$

The coefficients resulting in equations 21, 22 and 24 and the expression $d\delta/dx$ are explained in Appendix C.

The equations 21 - 25 are solved with an explicit intermediate step procedure. As initial values, values for θ_{11}, H_s, β, and u_e are inserted and the distribution of the displacement thickness δ_x is prescribed as a function of x.

1.3 Comparison with Measurements

Van den Berg and Elsenaar [19] have measured the development of a turbulent boundary layer on a crabbing plate (sweep angle 35°) in the range of low velocity. The wind tunnel wall above the plate was designed in such a manner that the generated pressure increase was large enough to cause boundary layer separation. Moreover, the attempt was made to approximate as closely as possible the conditions of the infinitely long, crabbing wing by the form of the end plates on the measurement plate.

The measured velocity profiles v/v_e are plotted in Figure 2 over the surface distance z standardized with the boundary layer thickness δ. Flow separation was observed near the measuring point 8 in the experiment. As can be seen in Figure 2, the requirement made for the calculation procedure that the velocity profile in the y direction can be approximated by the velocity profiles at the flat plate (drawn line) is confirmed here by the measurement results. In the adjacent, separating and separated range, the v/v_e profiles are sufficiently well represented by profiles at the flat plate. /15

The upper diagram in Figure 3 shows the measured quantities of δ_x^*, employed as input for the inverse procedure (the drawn line is the curve fit employed for the input). In the lower portion, the displacement thickness of the main flow profile δ_1^* has been compared with the measurements. The calculation results are a good representation of the measured quantities δ_1^*. A comparable good quality of

calculation for the quantities θ_{11}, θ_{12}, θ_{22} and δ_2^* is given in the Figures 4 and 5. Figure 6 shows the boundary layer thickness δ and the surface flow line angle β.

The form parameter H (relationship of displacement thickness to the momentum loss thickness) of the velocity profiles in the direction of main flow H_s, in the x direction H_x and in the y direction H_y are shown in Figure 7. The assumption is again confirmed here that there is a plate boundary layer velocity profile in the y direction. For this case, $H_y = 1.29$. For the entire area, the measurement also shows a constant value for H_y, corresponding approximately to the said value of 1.29. The comparison of measurement and calculation of the values for H_s and H_x is very satisfactory.

The measured and calculated values of the surface shearing force components c_{fx}, c_{fy} and c_{fs} are shown. The value $c_{fx} \equiv 0$ indicates separation at an infinitely long, crabbing wing by definition. As can be seen, the calculated separation point is situated in the area of the experimentally observed separation. /16

In Figure 9, the finally desired results of the inverse boundary layer calculation for the external velocity component u_e and the angle α have been compared with the measured quantities. Three different interpretation possibilities for the measured external velocity data can be given: 1. u_e and α measured, 2. u_e measured and α calculated from the condition of infinitely long, crabbing wing and 3. u_e and α calculated from the measured surface pressure distribution with the condition of infinitely long, crabbing wing. As can be seen, slight differences between the different representation possibilities only result near the separation point. The calculation provides a good agreement for the values of u_e and α. The calculation results are very closely situated to the quantities, derived from the measured wall thickness.

2. Expansion of the Integral Method on the Calculation of Three-Dimensional, Turbulent Boundary Layers to Adiabatic, Compressible Flows /17

Symbols

a	Speed of sound
$\bar{c}_f$	Transformed surface coefficient of friction
$\bar{F}$	Transformed entrainment coefficient
M	Mach number
T	Static temperature
T*	Reference temperature
z	Surface distance in the physical space

Z	Surface in the transformed space
γ	Ratio of the specific heats
$\bar{\delta}$	Transformed boundary layer thickness
$\bar{\delta}_1^* = \int_0^{\bar{\delta}} (1 - \frac{U}{U_e})\, dZ$	Transformed displacement thickness of the velocity profiles in the direction of main flow
$\bar{\delta}_2^* = -\int_0^{\bar{\delta}} \frac{V}{U_e}\, dZ$	Transformed displacement thickness of the velocity profile in the direction of transverse flow
$\bar{\theta}_{11} = \int_0^{\bar{\delta}} \frac{U}{U_e} (1 - \frac{U}{U_e})\, dZ$	Transformed momentum loss thickness of the velocity profile in the direction of main flow

Index /18

e	At the outer edge of the boundary layer
o	Reference state

2.1 Introduction

In the reference [20] there is a calculation method developed at Dornier described for three-dimensional, incompressible, turbulent boundary layers. This procedure is a further development and improvement of an existing procedure developed by Myring [21]. The differences to the work of Myring are:

1. The single parameter exponent profile for describing the velocity distribution in the direction of main flow has been replaced by double-parameter Cole profiles [12]. The surface friction parameter describes the velocity distribution near the surface and the pressure gradient parameter determines the velocity distribution in the external section of the boundary layer.

2. The empirical information on the surface coefficient of friction additionally required in using exponential profiles is not required.

3. Instead of the entrainment method employed by Myring in which the entrainment coefficient is determined directly as a function of the form parameter, a "lag entrainment" method has been utilized in the present method, taking into consideration the unbalance effects of the boundary layer.

In the following, the alterations are described for expanding the /19 procedure to the calculation of adiabatic, compressible flows.

2.2 Fundamentals

The effects of compressibility on the boundary layer development are taken into consideration by the Stewartson-Illingworth transformation

$$dz = \frac{\rho}{\rho_o} \frac{a_e}{a_o} dz \qquad (26)$$

The calculation procedure is limited to adiabatic flows and mach numbers $M \leq 2$. With the example of the transformed momentum loss thickness of the main flow profile

$$\bar{\theta}_{11} = \int_o^{\bar{\delta}} \frac{U}{U_e} \left(1 - \frac{U}{U_e}\right) dz$$

in which the thickness ρ no longer appears, the relationship between the compressible and the transformed, incompressible quantities is demonstrated.

Utilizing equation 26, it can be shown that

$$\theta_{11} = \int_o^{\delta} \frac{\rho U}{\rho_e U_e} \left(1 - \frac{U}{U_e}\right) dz = \frac{\rho_o}{\rho_e} \frac{a_o}{a_e} \int_o^{\bar{\delta}} \frac{U}{U_e} \left(1 - \frac{U}{U_e}\right) dz = \frac{\rho_o a_o}{\rho_e a_e} \bar{\theta}_{11}$$

$$\text{or} \qquad \bar{\theta}_{11} = \frac{\rho_e\, a_e}{\rho_o\, a_o}\,\theta_{11} = \xi\,\theta_{11} \tag{27}$$

where $$\xi = \left(\frac{T_e}{T_o}\right)^{\omega}$$

$$\omega = \frac{1}{2} + \frac{1}{\gamma - 1} = 3$$

and $$\frac{T_e}{T_o} = \left(1 + \frac{\gamma-1}{2} M_e^{\,2}\right)^{-1} \text{ ist.}$$

Equation 27 can also be written in the same manner for the momentum loss thicknesses

$$\begin{aligned} \bar{\theta}_{12} &= \xi\,\theta_{12} \\ \bar{\theta}_{21} &= \xi\,\theta_{21} \\ \bar{\theta}_{22} &= \xi\,\theta_{22} \end{aligned} \tag{28}$$

and for the displacement thickness of the transverse flow profile

$$\bar{\delta}_2^{*} = \xi\,\delta_2^{*} \tag{29}$$

When the quadratic temperature-velocity ratio and the condition dp/dz = 0 is utilized, the following formulation can be made:

$$\frac{T}{T_e} = \frac{\rho_e}{\rho} = 1 + \frac{\gamma-1}{2} M_e^{\,2}\left[1 - \left(\frac{U}{U_e}\right)^2 - \left(\frac{V}{U_e}\right)^2\right] \tag{30}$$

With equations 26 and 30, the result for the displacement thickness of the main flow profile δ_1^{*} /21

$$\delta_1^{*} = \xi^{-1}\left[\bar{\delta}_1^{*} + \frac{\gamma-1}{2} M_e^{\,2}\left(\bar{\delta}_1^{*} + \bar{\theta}_{11} + \bar{\theta}_{22}\right)\right] \tag{31}$$

and for the boundary layer thickness

$$\delta = \xi^{-1} \left[\bar{\delta} + \frac{\gamma-1}{2} M_e^2 \left(\bar{\delta}_1^* + \bar{\theta}_{11} + \bar{\theta}_{22}\right)\right] \tag{32}$$

The coefficient of friction c_{fx} can be written with the aid of the Eckert reference temperature concept

$$c_{fx} = \bar{c}_f \frac{T_e}{T^x} \tag{33}$$

with

$$\frac{T_e}{T^x} = 1 + 0.13 M_e^2 \tag{34}$$

The entrainment coefficient F can be given in the same manner according to a proposal by Horton [18]

$$F = \bar{F} \frac{T_e}{T^x} \tag{35}$$

In the derivation of the boundary layer equations in the transformed space, the following conversion has been utilized

$$\xi \frac{\partial \Theta_{11}}{\partial x} = \frac{\partial \bar{\Theta}_{11}}{\partial x} - \frac{\bar{\Theta}_{11}}{\xi} \frac{\partial \xi}{\partial x} = \frac{\partial \bar{\Theta}_{11}}{\partial x} + 3 (\gamma-1) M_e^2 \frac{\bar{\Theta}_{11}}{U_e} \frac{\partial U_e}{\partial x}$$

with similar expressions for

$$\frac{\partial \Theta_{21}}{\partial x}, \frac{\partial \Theta_{12}}{\partial y} \text{ und } \frac{\partial \Theta_{22}}{\partial y} .$$

With the exception that the velocity profiles in the transformed states can be represented by those of the incompressible flow, the resulting equations are expressed as: /22

x-impulse equation

$$\frac{1}{h_1}\frac{\partial \bar{\Theta}_{11}}{\partial x} + \bar{\Theta}_{11}\left\{\frac{1}{h_1 U_e}\frac{\partial U_e}{\partial x}\left[2-M_e^2\,(1-3\{\gamma-1\})\right] + \frac{1}{q}\frac{\partial}{\partial x}\left(\frac{q}{h_1}\right) + a_1\right\}$$

$$+ \frac{1}{h_1}\frac{\partial \bar{\Theta}_{12}}{\partial y} + \bar{\Theta}_{12}\;\frac{1}{h_2 U_e}\frac{\partial U_e}{\partial y}\left[2-M_e^2(1-3\{\gamma-1\})\right] + \frac{1}{q}\frac{\partial}{\partial y}\left(\frac{q}{h_2}\right) + a_3\} \qquad (36)$$

$$+ \bar{\Delta}_1^*\left\{\frac{1}{h_1}\frac{1}{U_e}\frac{\partial u_e}{\partial x} + a_1\frac{u_e}{U_e}\right\} + \bar{\Delta}_2^*\left\{\frac{1}{h_2}\frac{1}{U_e}\frac{\partial u_e}{\partial y} + a_2\frac{v_e}{U_e} + a_3\frac{u_e}{U_e}\right\}$$

$$+ \bar{\Theta}_{22}\,a_2 = \xi\frac{T_e}{T^*}\frac{\bar{c}_{fx}}{2}$$

y-impulse equation:

$$\frac{1}{h_1}\frac{\partial \bar{\Theta}_{21}}{\partial x} + \bar{\Theta}_{21}\left\{\frac{1}{h_1 U_e}\frac{\partial U_e}{\partial x}\left[2-M_e^2\,(1-3\{\gamma-1\})\right] + \frac{1}{q}\frac{\partial}{\partial x}\left(\frac{q}{h_1}\right) + b_3\right\}$$

$$+ \frac{1}{h_1}\frac{\partial \bar{\Theta}_{22}}{\partial y} + \bar{\Theta}_{22}\left\{\frac{1}{h_2 U_e}\frac{\partial U_e}{\partial y}\left[2-M_e^2\,(1-3\{\gamma-1\})\right] + \frac{1}{q}\frac{\partial}{\partial y}\left(\frac{q}{h_2}\right) + b_2\right\} \qquad (37)$$

$$+ \bar{\Delta}_1^*\left\{\frac{1}{h_1 U_e}\frac{\partial v_e}{\partial x} + b_1\frac{u_e}{U_e} + b_3\frac{v_e}{U_e}\right\} + \bar{\Delta}_2^*\left\{\frac{1}{h_2 U_e}\frac{\partial v_e}{\partial y} + b_2\frac{v_e}{U_e}\right\}$$

$$+ \bar{\Theta}_{11}\,b_1 = \xi\frac{T_e}{T^*}\frac{\bar{c}_{fy}}{2}$$

surface friction equation

/23

$$\frac{\partial \bar{\delta}}{\partial x} + \left(\frac{1}{\bar{\sigma}} + \frac{k}{\bar{\sigma}^2}\right)\bar{\delta}\frac{\partial \bar{\sigma}}{\partial x} + 2\,\bar{\delta}\frac{\partial \bar{\Pi}}{\partial x} = -\frac{\bar{\delta}}{U_e}\left[\frac{\partial U_e}{\partial x} + \frac{h_1}{h_2}\frac{v_e}{u_e}\frac{\partial U_e}{\partial y}\right]$$

$$- \frac{h_1}{h_2}\frac{v_e}{u_e}\left[\frac{\partial \bar{\delta}}{\partial y} + \left(\frac{1}{\bar{\sigma}} + \frac{k}{\bar{\sigma}^2}\right)\bar{\delta}\frac{\partial \bar{\sigma}}{\partial y} + 2\,\bar{\delta}\frac{\partial \bar{\Pi}}{\partial y}\right] \qquad (38)$$

entrainment equation:

$$\frac{1}{h_1 U_e}\frac{\partial}{\partial x}(\delta U_e \psi_1) + \frac{1}{h_2 U_e}\frac{\partial}{\partial y}(\delta U_e \psi_2) + \frac{\delta\psi_1}{q}\frac{\partial}{\partial x}\left(\frac{q}{h_1}\right) + \frac{\delta\psi_2}{q}\frac{\partial}{\partial y}\left(\frac{q}{h_2}\right)$$

$$- \frac{1}{h_1}\delta\psi_1 \frac{Me^2}{U_e}\frac{\partial U_e}{\partial x}[1 - 3(\gamma-1)] - \frac{1}{h_2}\delta\psi_2 \frac{Me^2}{U_e}\frac{\partial U_e}{\partial y}[1 - 3(\gamma-1)]$$

$$= \xi \frac{T_e}{T^*}\bar{F} \qquad (39)$$

lag-entrainment equation:

$$\frac{\partial \bar{F}}{\partial x} = h_1 \frac{U_e}{u_e}\left[\frac{\partial \bar{F}}{\partial s} - \frac{1}{h_2}\frac{v_e}{U_e}\frac{\partial \bar{F}}{\partial y}\right] \qquad (40)$$

with

$$\frac{\partial \bar{F}}{\partial s} = \frac{1}{\delta}(\bar{F}_{Eq} - \bar{F})$$

and

$$\bar{F}_{Eq} = \frac{.122}{(H_1 - 2.3)^{1.38}} \qquad (41)$$

The three-dimensional displacement thickness δ^* in the physical space is calculated with /24

$$\frac{\partial}{\partial x}\left(\frac{\rho_e q u_e \delta^*}{h_1}\right) + \frac{\partial}{\partial y}\left(\frac{\rho_e q v_e \delta^*}{h_2}\right) = \frac{\partial}{\partial x}\left(\frac{\rho_e q U_e \Delta_1^*}{h_1}\right) + \frac{\partial}{\partial y}\left(\frac{\rho_e q U_e \Delta_2^*}{h_2}\right) \qquad (42)$$

The quantities occurring in equations 36-42 are defined in reference [20]. The desired quantities in the physical space, e.g. θ_{11}, are determined with the aid of equation 3 from the calculated quantities in the transformed space, $\bar{\theta}_{11}$.

2.3 Results

The boundary layer measurements in a supersonic jet carried out by Hall and Dickens [22] have been recalculated. The shape of the supersonic jet, the course of the flow lines A, B and C and the Mach number distribution along the flow line B are presented in Figure 10. Figure 11 presents the results of the quantities θ_{11}, $\overline{H}$ and β. A comparison with the calculated results of the procedure by P. D. Smith [23] is also indicated.

A further calculation result of the procedure described here has already been presented in the report of the workshop on three-dimensional turbulent boundary layers [24]. Figure 12 shows the foundation shape of the wing. Figures 13 and 14 present the pressure distributions for a flow approach mach number of $M_\infty = 0.5$ and an angle of inclination of 0 or 8°. Figures 15 and 16 present the calculated results of the present procedure (complete circles) compared to the average result of all calculation procedures participating in the workshop (three integral procedures and five difference procedures).

3. Pressure Distribution Calculations with Three-Dimensional, Transsonic Wings, Taking into Consideration the Friction Effects /25

3.1 Introduction

The alteration work in boundary layer procedures for the approximate calculation of separation areas have been undertaken within the framework of the present commission. Results of this work have also been presented in the ZKP report, Dornier Report No. 79/38B.

In order to calculate the frictionless flow around three-dimensional wings in the transsonic range, the small perturbation procedure [25] is utilized. The development of the three-dimensional boundary layer is determined with an integral procedure [20,26]. Iterative calculations of the frictionless flow and flow subjected to friction, using the "displacement surface concept", produce the pressure distribution in the converged state while taking into consideration the effects of friction.

3.2 Approximate Determination of Boundary Layer Quantities in the Case of Separation

When laminar separation occurs in the calculation before achieving the defined conversion point, the calculation is continued with the condition of an adjacent, turbulent boundary layer. In the case of the turbulent boundary layer separation, no further data can be determined downstream from the separation point with the available method.

To avoid interruption of the cycle of the iterative, frictionless /26 and friction calculation, the following, approximate determination of is applied, see Figure 17.

If a turbulent separation occurs in the calculation in the wing section y_{n+4} at the percent line x_n, the wing section y_{n+4} is excluded from the normal calculation. In the wing sections $y_{n+3} + y_{n+5}$, boundary conditions for the remaining areas of the three-dimensional calculation are determined by assuming the condition of the infinitely long, crabbing wing in these wing sections. Finally, after further integration in the x direction, separation in the wing sections $y_{n+2} \div y_{n+6}$ is determined.

These wing sections are now excluded from the normal calculation and boundary conditions for the remaining areas of the three-dimensional calculation are determined in the wing sections y_{n+1} and y_{n+7}. In this manner, a separation line can be calculated in the case of three-dimensional wing boundary layers. In the wing sections excluded from the normal calculation, the boundary layer development is determined in an approximation. In order to calculate the desired displacement thickness in this case, only the entrainment equation is employed with a defined form parameter of the boundary layer, corresponding to a separated turbulent boundary layer. Moreover, the value of the surface flow line angle determined at the separation point is maintained. For this reason, the solution of the x and y-impulse integral equations is not required.

3.3 Example Calculations with Wings /27

3.3.1 PT7 Wing

The fundamental shape of the PT7 wing, developed and measured by the FFA in Stockholm, is shown in Figure 18. The results of the calculations are compared in wing sections $1 \div 3$ with measurements at a mach number of 0.9 and a Reynolds number of $1.38 \cdot 10^7$ [1/m]. Figure 19 shows the three-dimensional displacement thickness in wing section 2 related to the root wing depth, plotted over the relative wing depth x/C for a pure turbulent flow. Curve 1 corresponds to the boundary layer calculation with the first frictionless pressure distribution. The results are smoothed and only 15% of the determined displacement thickness are transmitted to the second frictionless calculation. The results of the second boundary layer calculation, curve 2, are again smoothed and 80% of the displacement thickness transmitted. After the third boundary layer calculation, smoothing is no longer carried out and 100% of the displacement thickness are employed. The fifth subsequent calculation did not demonstrate any deviations compared to the fourth, and the result was considered as converged.

As can be seen, turbulent separation occurs in the first boundary layer calculation at a 85% wing depth. The values of δ^* for $x/c > .85$ correspond to the above-described calculated approximation. In the second boundary layer calculation, the frictionless pressure distribution was altered in such a manner that separation no longer occurred.

For comparison, the converged result for a boundary layer flow is drawn (dotted line), for which up to 20% wing depth a laminar flow was assumed.

The Figures 20-22 show the pressure distributions determined by calculation in the wing sections 1 ÷ 3 in comparison to the measurements. In all wing sections, a marked upstream motion of the area of pressure increase is determined on the upper side of the wing. In the wing sections 1 and 2, the pressure distribution remains almost unaltered in front of the area of pressure increase, only in the wing section 3 can a clear reduction in the under pressure level be determined. /28

The rear edge pressure on the lower side of the wing is reduced in all sections.

Figure 23 shows the comparison of the converged pressure distribution in the case of pure turbulence and a laminar-turbulent boundary layer flow. In the pure turbulent case, the area of pressure increase is shifted more greatly upstream, explained by the fact that the interaction between boundary layer and external flow becomes more intensive in the case of larger boundary layer thicknesses.

Figure 24 shows the separation areas on the wing, resulting in the course of the iterations. It becomes clear that the separation area has become very much smaller in the converged case than in the first subsequent calculation. This result underlines the practicality of the approximate determination of boundary layer in the "separated" area, 3.1.

3.3.2 ZKP Wing /29

Figure 25 shows the basic form of the wing for the ZKP wing. The displacement thickness for the wing section 2 is shown in Figure 26 in the course of the iterative calculations. Figures 27-29 show the measured pressure distributions and those determined in calculations. The comparison shows clear deviations between measurement and calculation, partially attributable to elastic shaping of the wing and perhaps to the course grid employed in the frictionless case.

4. Laminar Boundary Layers in Tipped Rotation Ellipsoids /30

4.1 Introduction

A detailed description of this work can be found in reference [27]. The calculation results shown here are determined with the Dornier integral procedure for calculating three-dimensional, laminar boundary layers [26].

4.2 Results

The frictionless external flow is determined with a potential, theoretical method. The lateral ratio of the observed ellipsoid was 6:1 and the angle of inclination $\alpha = 10^{\circ}$.

The calculation results are compared in Figure 30 with those of a difference procedure [28]. $\bar{\theta}_{11}$ and $\bar{\delta}_1^*$ are the momentum loss thicknesses or displacement thickness of the velocity profile in the direction of the main flow, $\bar{T}_w$ is the resulting surface shearing force and β the surface streamline angle.

As Figure 30 shows, the results of the integral procedure are in good agreement with those of the difference procedure.

The Figures 31 and 32 show results for the surface shearing force τ_w in comparison with measurements [29] and results of difference procedures.

The development of the three-dimensional displacement thickness δ^* is shown in the Figures 33 and 34. Figure 35 describes the course of the surface streamlines. The vectors drawn in indicate the direction of the resulting surface shearing force. The calculated turbulence departure lines are shown in the Figures 36-38 and compared with the results of the difference procedure. /31

5. Summary /32

5.1 Inverse Integral Procedure

An inverse boundary layer integral procedure has been developed for calculating separated, turbulent boundary layers with infinitely long, crabbing wings. The displacement thickness distribution of the velocity profile in the direction perpendicular to the leading edge of the wing is employed as input. The velocity distribution is calculated according to size and direction at the outer edge of the boundary layer.

The expanded double-parameter profile family of Coles is employed for describing the velocity profile in the direction of wing flow. It is assumed that the velocity profile v/v_e in a direction parallel to the leading edge of the wing corresponds to that on a flat plate.

The entrainment equation is employed with a lag-entrainment method for calculating the entrainment coefficient, the surface friction equation is employed for determining the surface shearing force component in the direction of main flow and a simple relationship is employed for determining the surface shearing force component in the direction parallel to the leading edge of the wing in order to solve the problem in the x-impulse integral equation.

A comparison with measurements in a separated, turbulent boundary layer confirms the assumption made on the v/v_e velocity profile.

Moreover, the quality of agreement demonstrates the usefulness of the calculation procedure.

5.2 Expansion of the Three-Dimensional, Turbulent Integral Procedure to Compressible Flows /33

The expansion of the existing integral procedure for three-dimensional, turbulent flows to compressible, adiabatic flows has been made with a compressibility transformation. The calculation examples show good agreement with measurements and other procedures.

5.3 Example Calculations with Wings

The iterative calculation of pressure distribution with three-dimensional transsonic wings while taking into consideration the effects of friction produce a satisfactory agreement between measurement and calculation. The usefulness of an approximation procedure for determining the boundary layer development in the case of separated, turbulent boundary layers has been demonstrated.

5.4 Laminar Boundary Layers with Tipped Ellipsoids

A comparison of the calculation results of laminar boundary layers in the case of tipped rotation ellipsoids of the Dornier integral procedure with available measurements (DFVLR) and difference procedures produced good agreement. Even the position of the turbulent departure lines at the ellipsoid has been calculated in very good agreement with the difference procedure.

Appendix A

Calculation of the integral quantities Θ_{11} and Δ_1^* from integral quantities in the s, n coordinate system.

It applies that

$$\frac{u}{U_e} = \frac{U}{U_e}\cos\alpha - \frac{V}{U_e}\sin\alpha \tag{1a}$$

$$\frac{v}{U_e} = \frac{U}{U_e}\sin\alpha + \frac{V}{U_e}\cos\alpha \tag{2a}$$

It results that

$$\Theta_{11} = \theta_{11}\cos^2\alpha - (\theta_{12} + \theta_{21})\sin\alpha\cos\alpha + \theta_{22}\sin^2\alpha \tag{3a}$$

$$\Delta_1^* = \delta_1^*\cos\alpha - \delta_2^*\sin\alpha \tag{4a}$$

The expression with equation 4 and 7 is

$$\theta_{11} = \delta\frac{\omega}{k}\left\{\left[\Pi\frac{|\omega|}{\omega} + 1\right] - \frac{\omega}{k}\left[1.5\,\Pi^2 + 3.1794\frac{|\omega|}{\omega}\Pi + 2\right]\right\} \tag{5a}$$

$$\theta_{12} = \mathrm{tg}\,\alpha\frac{\delta}{k^2}\{1.5\,\Pi^2\omega^2 - 0.031163\,\Pi|\omega| + 3.1794[\Pi\omega|\omega| - 0.01662(\Pi|\omega| + 0.625\,\omega)] + 2\omega(\omega - 0.03324)\} \tag{6a}$$

$$\theta_{22} = -\mathrm{tg}^2\alpha\frac{\delta}{k^2}\{1.5\,\Pi^2\omega^2 + 3.1794\,\Pi|\omega|\omega - 0.16801\,\Pi|\omega| + 2\omega^2 - 0.19901\,\omega + 0.00505\} \tag{7a}$$

$$\delta_1^* = \delta\frac{\omega}{k}\left[\Pi\frac{|\omega|}{\omega} + 1\right] \tag{8a}$$

$$\delta_2^* = -\frac{\delta}{k}\mathrm{tg}\,\alpha\left\{\omega\left[\Pi\frac{|\omega|}{\omega} + 1\right] - 0.05402\right\} \tag{9a}$$

For θ_{21} it applies that /40

$$\theta_{21} = \theta_{12} + \delta_2^* \tag{10a}$$

Appendix B /41

Calculation of the entrainment is related to integral quantities, similar to the procedure in [4], formed from the velocity distribution situated above the U = 0 line.

According to equation 4, it applies for the position z_0, at which U = 0

$$1 = \frac{\omega}{k}\left[\Pi \frac{|\omega|}{\omega}\left\{1 + \cos\left(\pi \frac{z_o}{\delta}\right) - \ln \frac{z_o}{\delta}\right]\right. \tag{16}$$

or

$$z_o = \delta \exp\left[\Pi \frac{|\omega|}{\omega}\left\{1 + \cos\left(\pi \frac{z}{\delta}\right) - \frac{k}{\omega}\right]\right. \tag{26}$$

It follows for the integral quantity with $\omega < 0$

$$\bar{\delta} = \delta - z_o \tag{3b}$$

$$\delta_1^* = \delta \frac{|\omega|}{k} \int_{z_o}^{1} \left[\Pi \left\{1 + \cos\left(\pi \frac{z}{\delta}\right)\right\} + \ln \frac{z}{\delta}\right] d\frac{z}{\delta} \tag{4b}$$

$$\delta_1^* = \delta \frac{|\omega|}{k}\left[\Pi \left\{1 - \frac{z_o}{\delta} - \frac{1}{\pi} \sin\left(\pi \frac{z_o}{\delta}\right)\right\} + \left(\frac{z_o}{\delta} - 1\right) - \frac{z_o}{\delta} \ln \frac{z_o}{\delta}\right]$$

$$\bar{\theta}_{11} = \delta \frac{|\omega|}{k} \int_{z_o\delta}^{1} \left[1 - \frac{|\omega|}{k}\left(\Pi \left\{1 + \cos\left(\pi \frac{z}{\delta}\right)\right\} + \ln \frac{z}{\delta}\right)\right]\left[\Pi \left\{1 + \cos\left(\pi \frac{z}{\delta}\right) + \ln \frac{z}{\delta}\right] d\frac{z}{\delta}\right.$$

$$\bar{\theta}_{11} = \bar{\delta}_s^* - \delta \frac{\omega^2}{k^2}\left[\left(1 - \frac{z_o}{\delta}\right)\left(1.5\,\Pi^2 - 4\Pi + 2\right) - 2 \frac{z_o}{\delta} \ln \frac{z_o}{\delta}\left(\Pi + 1\right)\right.$$

$$- \frac{z_o}{\delta}\left(\ln \frac{z_o}{\delta}\right)^2 - \frac{2}{\pi} \sin\left(\pi \frac{z_o}{\delta}\right) - \frac{1}{4\pi} \sin\left(2\pi \frac{z_o}{\delta}\right) + 2 \frac{\Pi}{\pi}\left(1.289\right.$$

$$\left.\left.\ln \frac{z_o}{\delta} \sin\left(\pi \frac{z_o}{\delta}\right) - \frac{\left(\pi \frac{z_o}{\delta}\right)^3}{18} + \frac{\left(\pi \frac{z}{\delta}\right)^5}{600} - \frac{\left(\pi \frac{z_o}{\delta}\right)^7}{35280} + \frac{\left(\pi \frac{z}{\delta}\right)^9}{3265920}\right]\right. \tag{5b}$$

Appendix C

For the components of the surface shearing force coefficient it applies that

$$c_{fx} = c_{fs} (\cos \alpha - \sin \alpha \tan \beta) \tag{1c}$$

$$c_{fy} = c_{fs} (\sin \alpha + \cos \alpha \tan \beta) \tag{2c}$$

Eliminating the value tan β from equation 1c and 2c,

$$c_{fx} = \frac{c_{fs}}{\cos \alpha} \left[1 - \frac{c_{fy}}{c_{fs}} \sin \alpha\right] \tag{3c}$$

The following derivations are to be formed for determining the coefficients in the equations 21, 22 and 24, where it applies for example that $\partial \theta_{11}/\partial \delta = \theta_{11_\delta}$

$$\theta_{11_\delta} = \frac{\theta_{11}}{\delta} \qquad \theta_{12_\delta} = \frac{\theta_{12}}{\delta} \tag{4c}$$

$$\theta_{21_\delta} = \frac{\theta_{21}}{\delta} \qquad \theta_{22_\delta} = \frac{\theta_{22}}{\delta}$$

$$\delta_{1_\delta}^* = \frac{\delta_1^*}{\delta} \qquad \delta_{2_\delta}^* = \frac{\delta_2^*}{\delta}$$

$$\theta_{11_\Pi} = \frac{\delta}{k} |\omega| - \delta \frac{\omega^2}{k^2} \left[3\Pi + 3.1794 \frac{|\omega|}{\omega}\right]$$

$$\theta_{12_\Pi} = \text{tg } \alpha \frac{\delta}{k^2} \{3\Pi \omega^2 + 3.1794 \omega |\omega| - 0.0840 |\omega|\}$$

$$\theta_{21_\Pi} = \theta_{12_\Pi} + \delta_{2_\Pi}^* \tag{5c}$$

$$\theta_{22_\Pi} = - \text{tg}^2 \alpha \frac{\delta}{k^2} \{3\Pi \omega^2 + 3.1794 |\omega| \omega - 0.16801 |\omega|\}$$

$$\delta_{1_\pi}^* = \frac{\delta}{k} |\omega|$$

$$\delta_{2_\pi}^* = -tg\ \alpha \frac{\delta}{k} |\omega|$$

$$\theta_{11_\omega} = \frac{\delta}{k} \{[\Pi \frac{|\omega|}{\omega} + 1] - 2 \frac{\omega}{k} [1.5\ \Pi^2 + 3.1794 \frac{|\omega|}{\omega} + 2]\}$$

$$\theta_{12_\omega} = tg\ \alpha \frac{\delta}{k^2} \{3\ \Pi^2\ \omega - 0.031163\ \Pi \frac{|\omega|}{\omega} + 3.1794\ [2\ \Pi^2\ |\omega| - 0.01662\ \Pi \frac{|\omega|}{\omega}]$$

$$+ 4\ \omega\}$$

$$\theta_{21_\omega} = \theta_{12_\omega} - \delta_{2_\omega}^*$$

$$\theta_{22_\omega} = -tg^2\ \alpha \frac{\delta}{k^2} \{3\ \Pi^2\ \omega + 6.3588\ \Pi\ |\omega| - 0.1681\ \Pi \frac{|\omega|}{\omega} + 4\ \omega - 0.19901\}$$

$$\delta_{1_\omega}^* = \frac{\delta}{k} \Pi \frac{|\omega|}{\omega} \qquad (6c)$$

$$\delta_{2_\omega}^* = -tg\ \alpha \frac{\delta}{k} \Pi \frac{|\omega|}{\omega}$$

For example, with $\theta_{11_u} = \partial\theta_{11}/\partial u_e$ and $\partial d/\partial U_e = -\sin\alpha \cos\alpha\ 1/U_e$ it results that

$$\theta_{11_u} = 0$$

$$\theta_{12_u} = -\frac{\theta_{12}}{u_e}$$

$$\theta_{21_u} = \theta_{12_u} + \delta_2^*{}_u$$

$$\theta_{22_u} = -2 \frac{\theta_{22}}{u_e}$$

$$\delta_1^*{}_u = 0$$

$$\delta_2^*{}_u = -\frac{\delta_2^*}{u_e}$$

When A is representative for δ, Π and ω, the result for the coefficients in equations 21, 22 and 24 is /45

$$\Theta_{11_A} = \theta_{11_A} \cos^2 \alpha - \{\theta_{12_A} + \theta_{21_A}\} \sin \alpha \cos \alpha + \theta_{22_A} \sin^2 \alpha \quad (8c)$$

$$\Delta^*_{1_A} = \delta^*_{1_A} \cos \alpha - \delta^*_{2_A} \sin \alpha \quad (9c)$$

For Θ_{11_u} and $\Delta^*_{1_u}$ the result is

$$\Theta_{11_u} = \theta_{11_u} \cos^2 \alpha - \{\theta_{12_u} + \theta_{21_u}\} \sin \alpha \cos \alpha - \theta_{22_u} \sin^2 \alpha + \sin^2 \alpha \cos^2 \alpha \frac{1}{u_e} [2\theta_{11} + (\frac{\cos^2 \alpha - \sin^2 \alpha}{\sin \alpha \cos \alpha})(\theta_{12} + \theta_{21}) - 2\theta_{22}] \quad (10c)$$

$$\Delta^*_{1_u} = \delta^*_{1_u} \cos \alpha - \delta^*_{2_u} \sin \alpha + \sin \alpha \cos \alpha \frac{1}{u_e} [\delta^*_1 \sin \alpha + \delta^*_2 \cos \alpha] \quad (11c)$$

The result for the coefficients ψ

$$\psi = \frac{u_e}{U_e} \delta - \Delta^*_1 \qquad \psi_\Pi = -\Delta^*_{1_\Pi}$$

$$\psi_\delta = \frac{u_e}{U_e} - \Delta^*_{1_\delta} \qquad \psi_\omega = -\Delta^*_{1_\omega} \quad (12c)$$

$$\psi_u = \frac{\delta}{U_e}(1 - \frac{u_e^2}{U_e^2}) - \Delta^*_{1_u}$$

and moreover

$$\phi_\Pi = 2\delta \frac{|\omega|}{\omega} \qquad \phi_\omega = \delta [\frac{k}{\omega^2} + \frac{1}{\omega}] \quad (13c)$$

The quantities P_i are defined as follows:

$$P_1 = 2\,\theta\,\frac{u_e}{U_e^2} + \frac{\Delta_1^*}{U_e} + \theta_u$$

$$P_2 = \psi\,\frac{u_e}{U_e^{22}} + \psi_u$$

$$P_3 = \delta\,\frac{u_e}{U_e^2}$$

For the derivation $\delta_{\Delta_1}{}^*$ it applies with

$$\delta_{\Delta_1}^* = \frac{\partial\delta}{\partial\Delta_1^*}$$

and equations 4a, 8a and 9a

$$\Delta_1^* = \frac{\delta}{k}\,\frac{1}{\cos\alpha}\,A$$

$$A = \omega\,(\Pi\,\frac{|\omega|}{\omega} + 1) - 0.05402\,\sin^2\alpha \qquad (14c)$$

$$\delta_{\Delta_1}^* = \frac{k}{A}\cos\alpha$$

For the derivation of the boundary layer thickness, it can be written as follows: /47

$$\frac{d\delta}{dx} = \delta_{\Delta_1}{}^*\,\frac{d\Delta_1^*}{dx} + \delta_\omega\,\frac{d\omega}{dx} + \delta_\pi\,\frac{d\Pi}{dx} + \delta_u\,\frac{d\,u_e}{dx} \qquad (15c)$$

with

$$\delta_\omega = -k\,\Delta_1^*\cos\alpha\,\frac{1}{A^2}\,(\Pi\,\frac{|\omega|}{\omega}+1)$$

$$\delta_\Pi = -k\,\Delta_1^*\cos\alpha\,\frac{1}{A^2}\,|\omega| \qquad (16c)$$

$$\delta_u = \frac{k\Delta_1^*}{A^2}\,\frac{\sin^2\alpha\cos\alpha}{u_e}\,(A - 0.10804\cos^2\alpha)$$

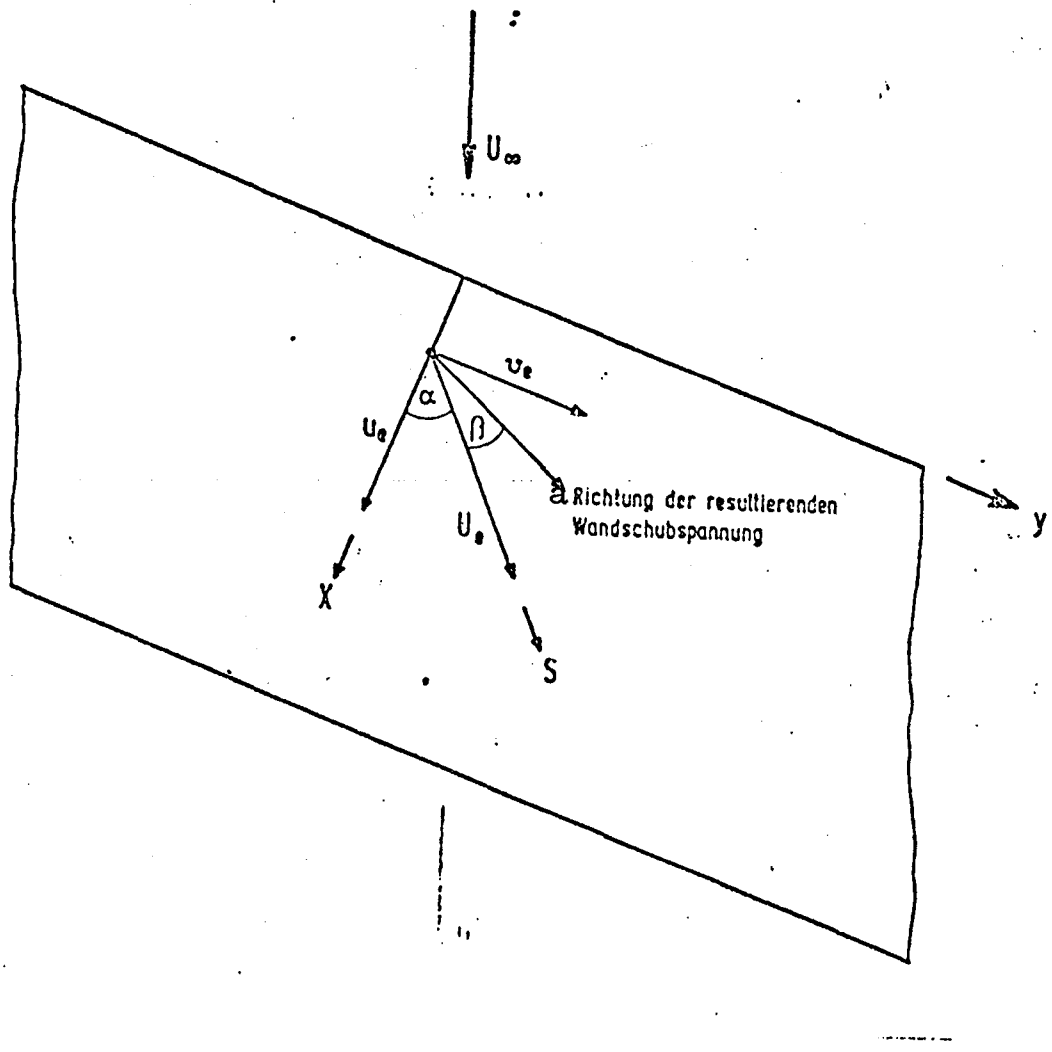

Fig. 1: Definition of the Velocity Components and the Angle α and β

Key: a. Direction of the resulting surface shearing force

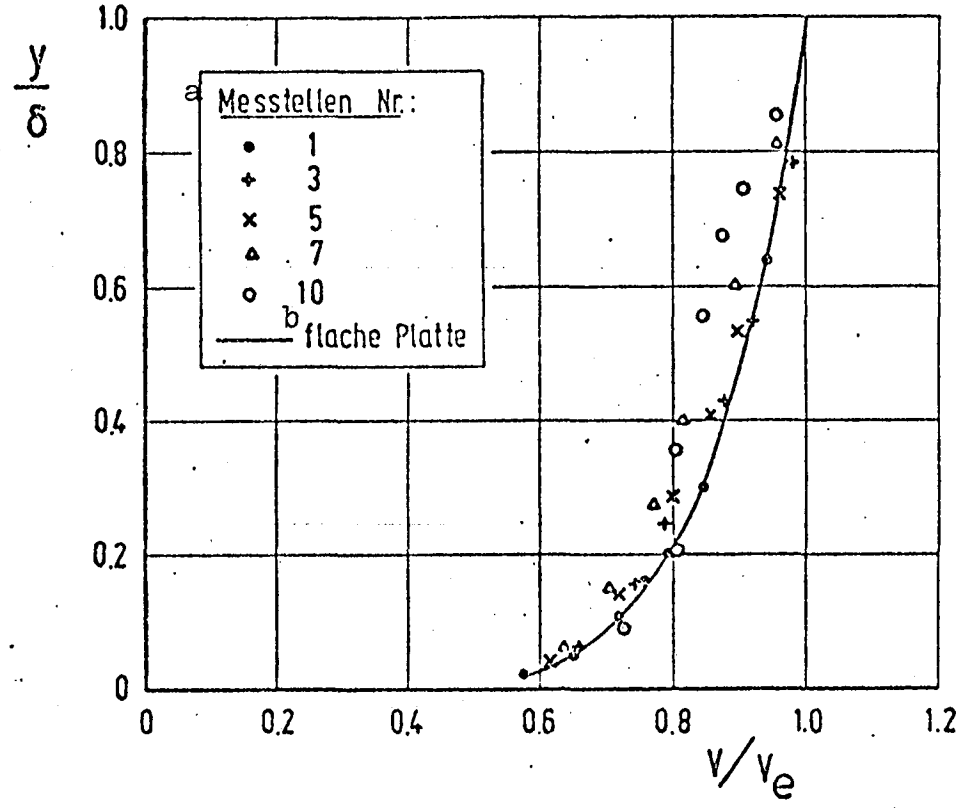

Fig. 2: Comparison of the measured turbulent velocity profile v/v_e with the velocity profile on a flat plate. [19]

Key: a. Measurement points no.
b. flat plate

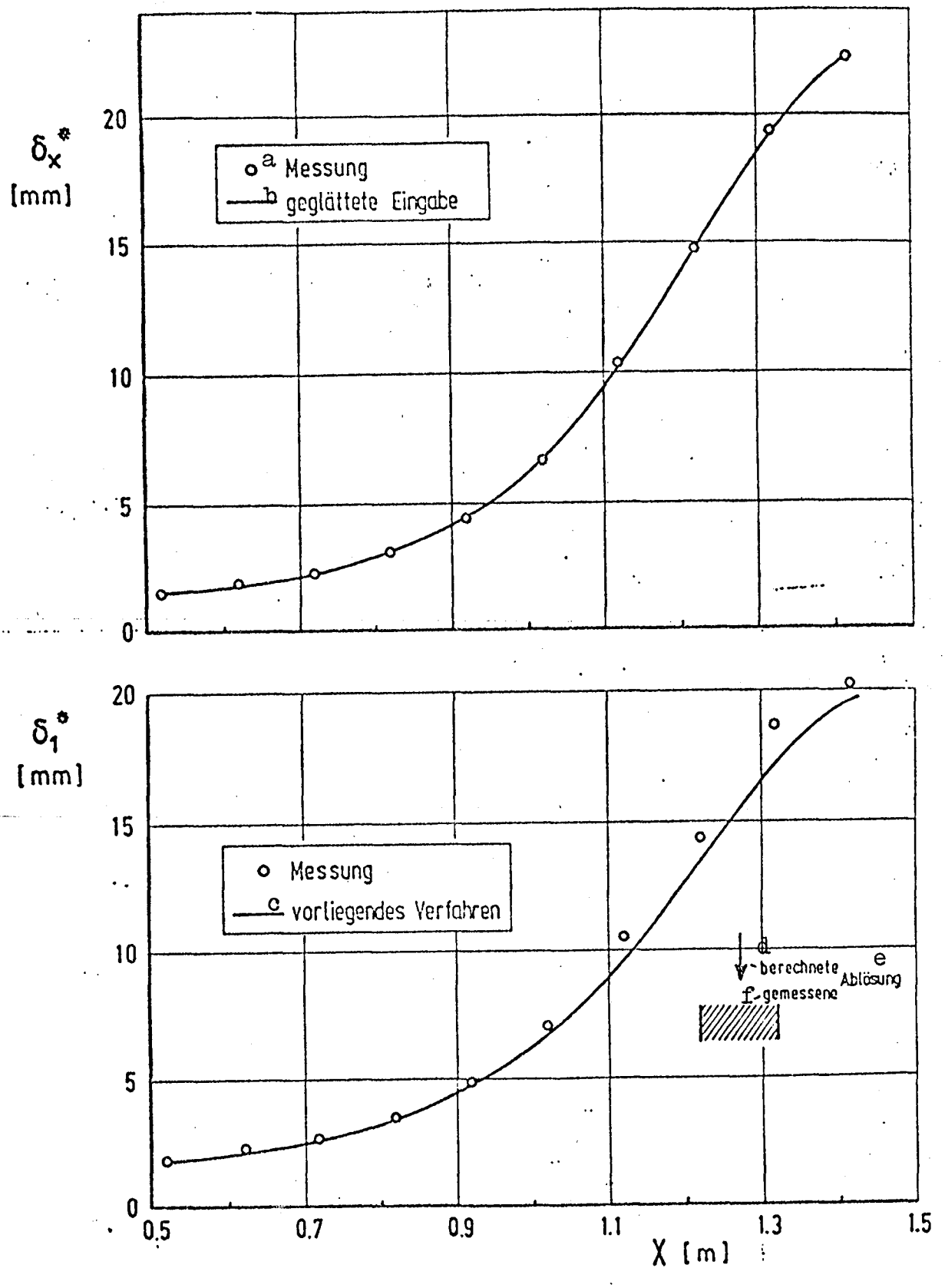

Fig. 3: Distribution of the measured quantity δ_x^* [19] as input and the comparison of the calculated quantity δ_1^* with the measurement [19] .

Key: a. measurement b. curve fit c. present procedure
d. calculated e. solution f. measured

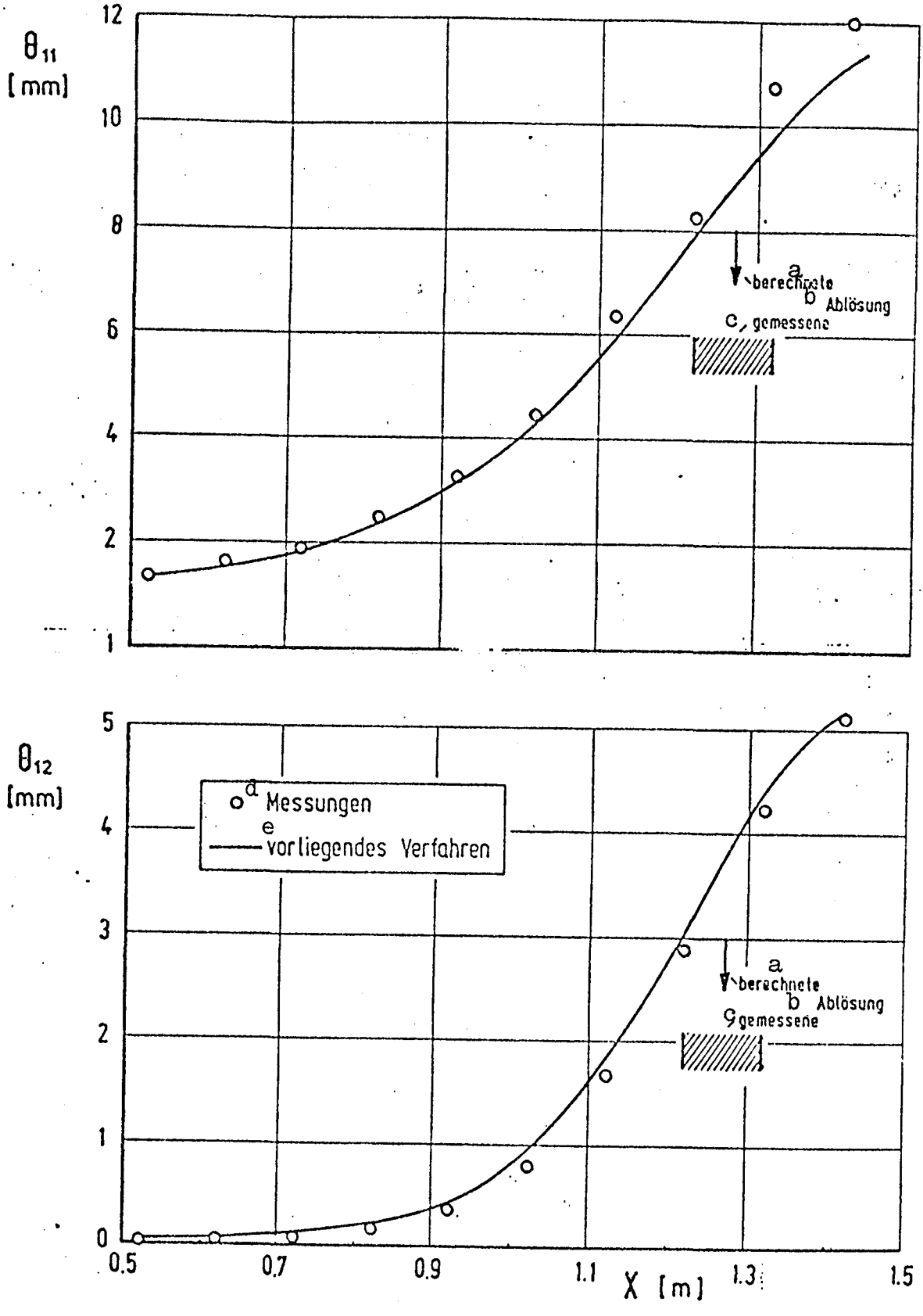

Fig. 4: Comparison of the calculated quantities θ_{11} and θ_{12} with the measurements [19].

Key: a. calculated b. separation c. measured
d. measurements e. present procedure

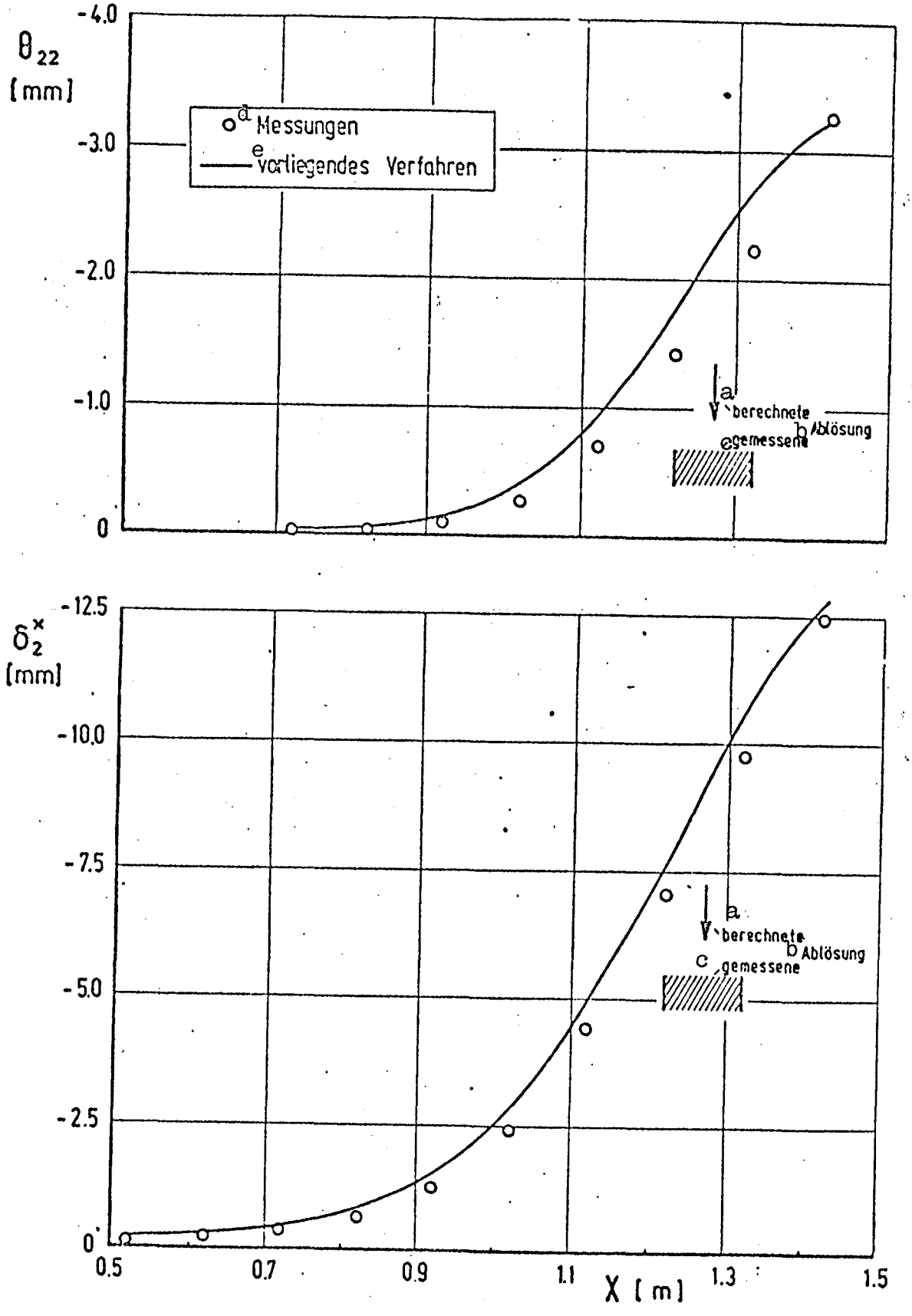

Fig. 5: Comparison of the calculated quantities θ_{22} and δ_2^* with the measurements [19].

See Fig. 4 for key.

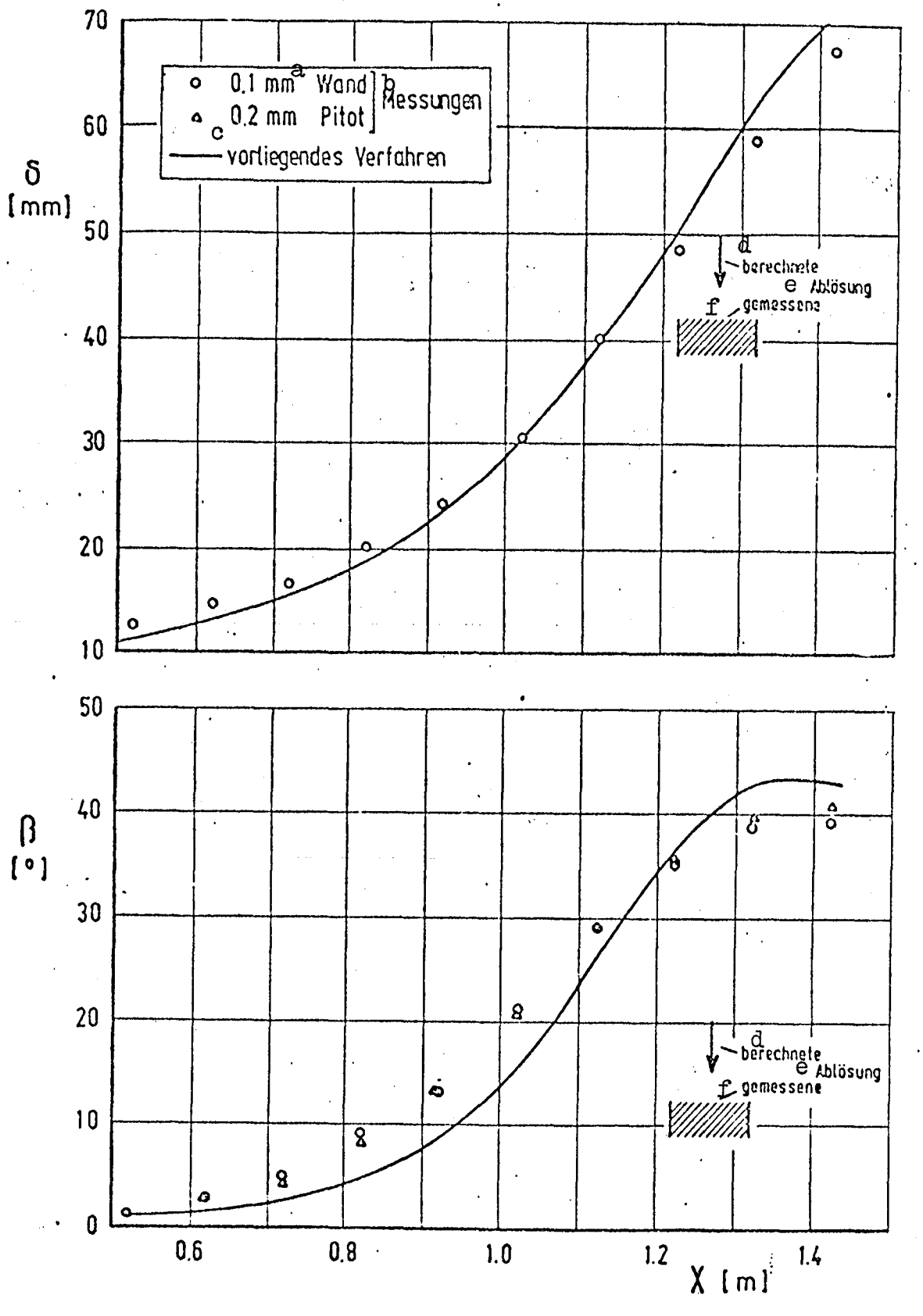

Fig. 6: Comparison of the calculated boundary layer thickness δ and the surface streamline angle β with the measurement [19].

Key:
a. surface
b. measurements
c. present procedure
d. calculated
e. separation
f. measured

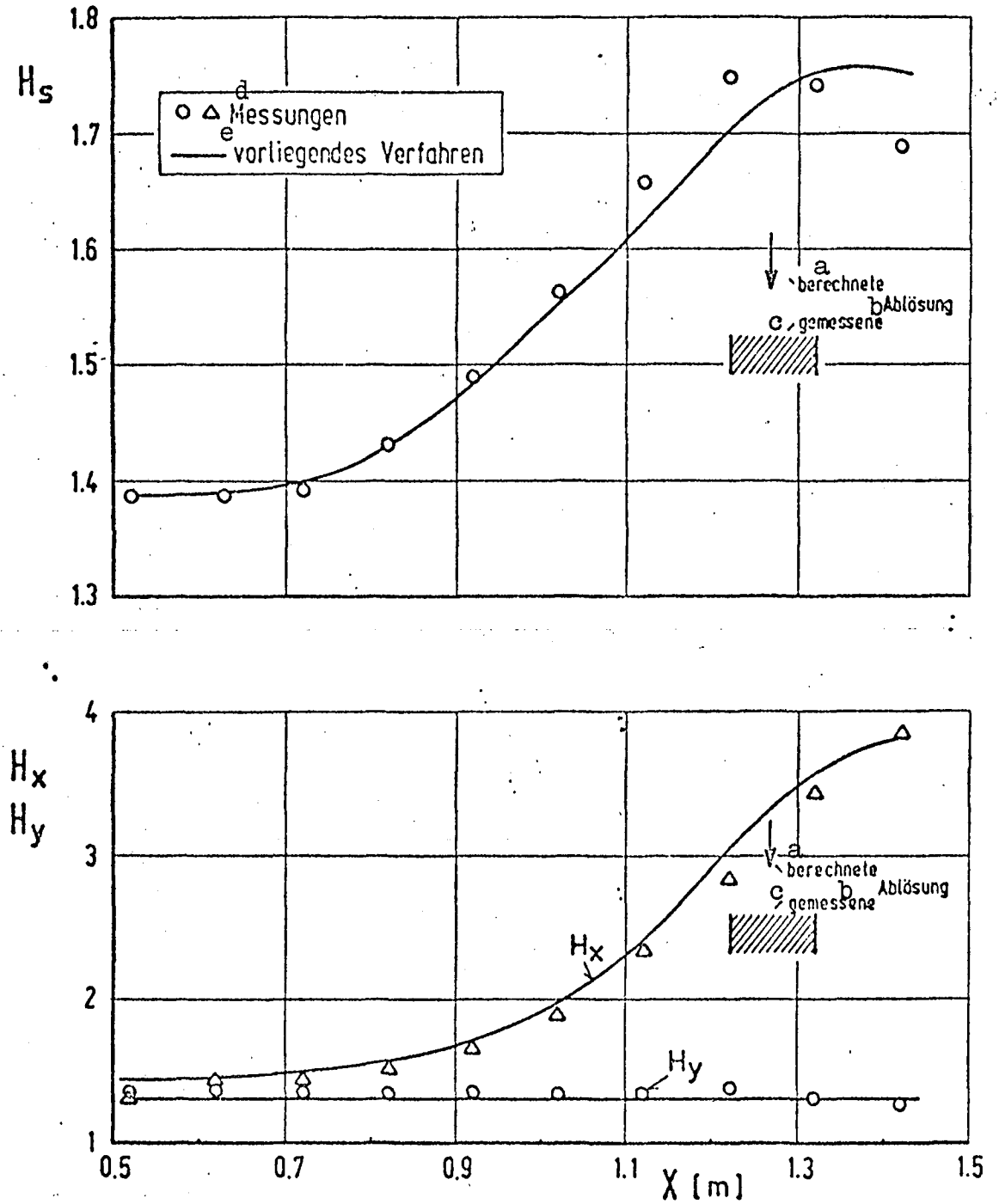

Fig. 7: Comparison of the calculated form parameters H_s, H_x and H_y with the measurements [19].

See Fig. 4 for key.

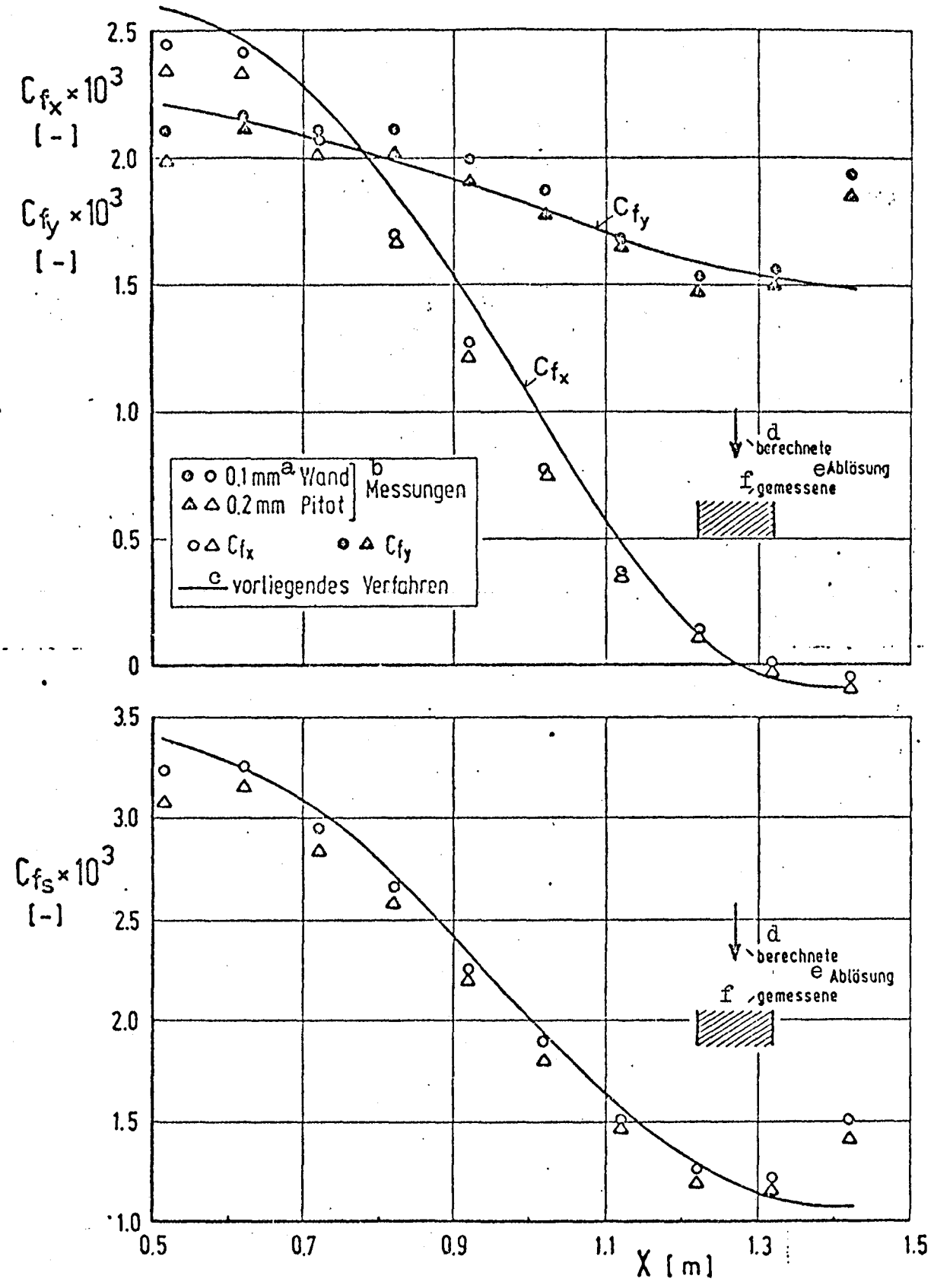

Fig. 8: Comparison of the calcuated shearing force coefficients cf_x, cf_y and cf_s with measurements.
See Fig. 6 for key.

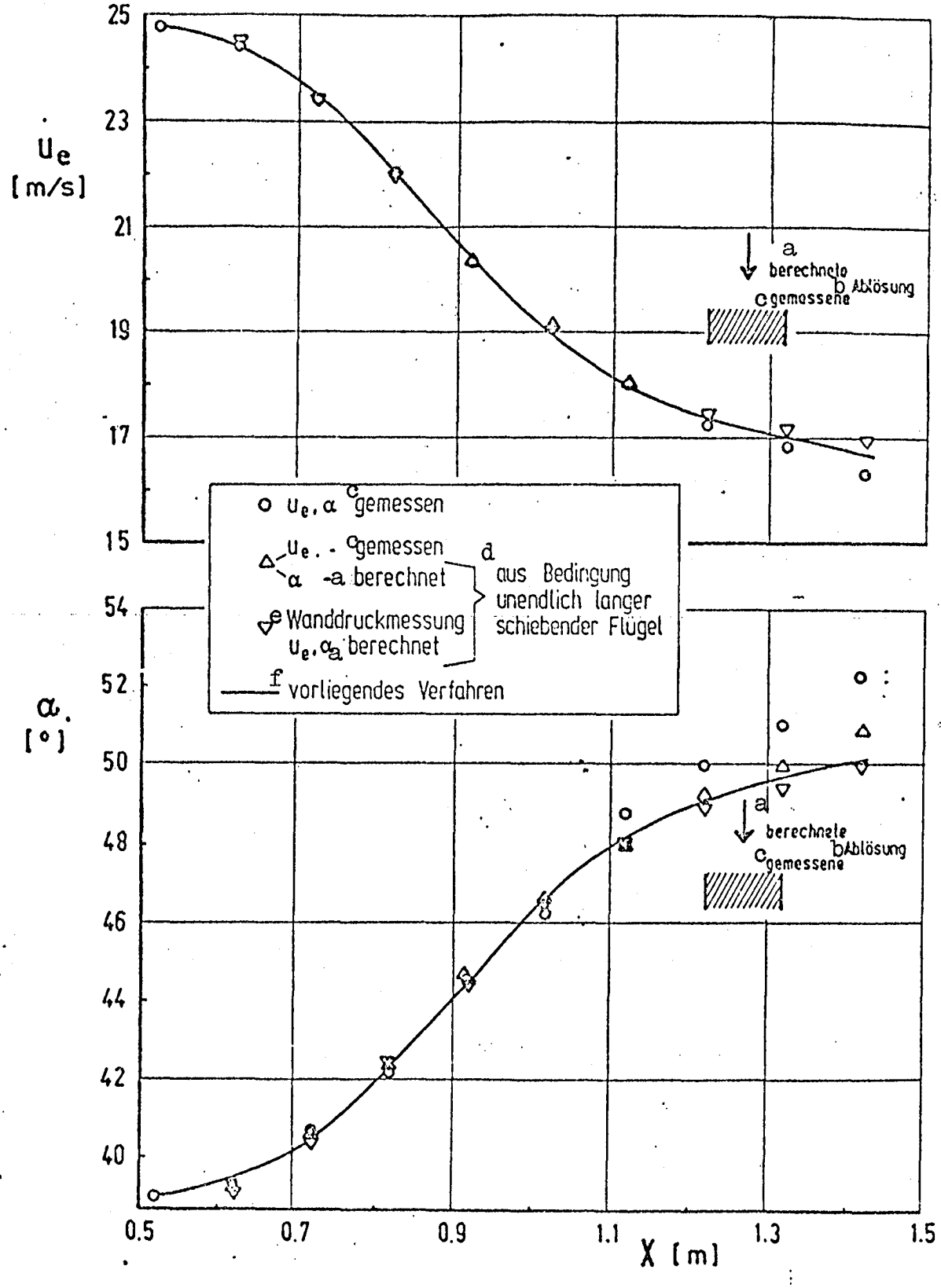

Fig. 9: Comparison of calculated values of the velocity component u_e and of the angle α with the measured values. [19]

Key: a. calculated
b. separation
c. measured
d. from the condition of infinitely long, crabbing wing
e. surface pressure measurement
f. present procedure

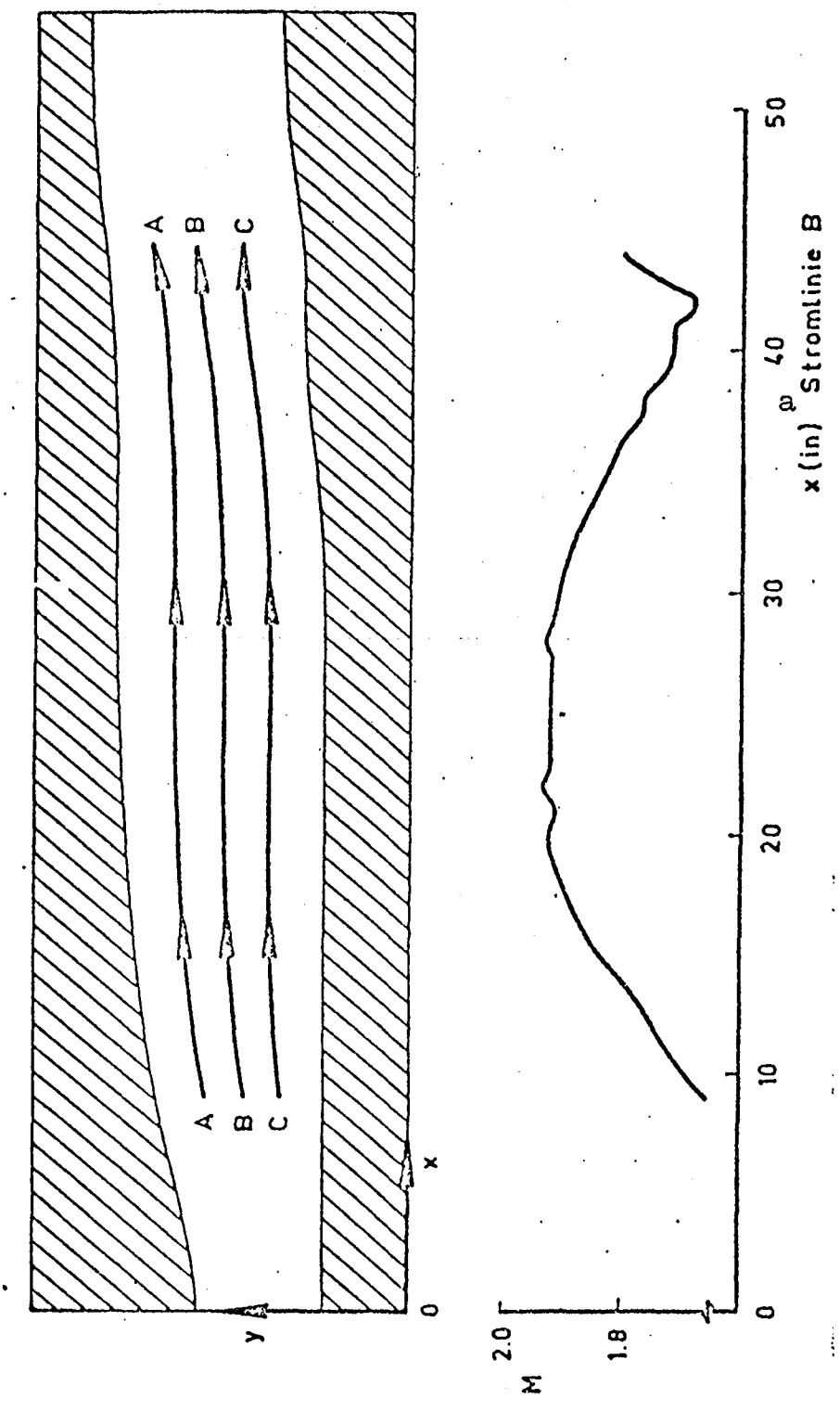

Fig. 10: Shape of the supersonic nozzle, course of the streamlines A, B, C and the mach number distribution along the streamline B in the experiment [22].

Key: a. streamline B

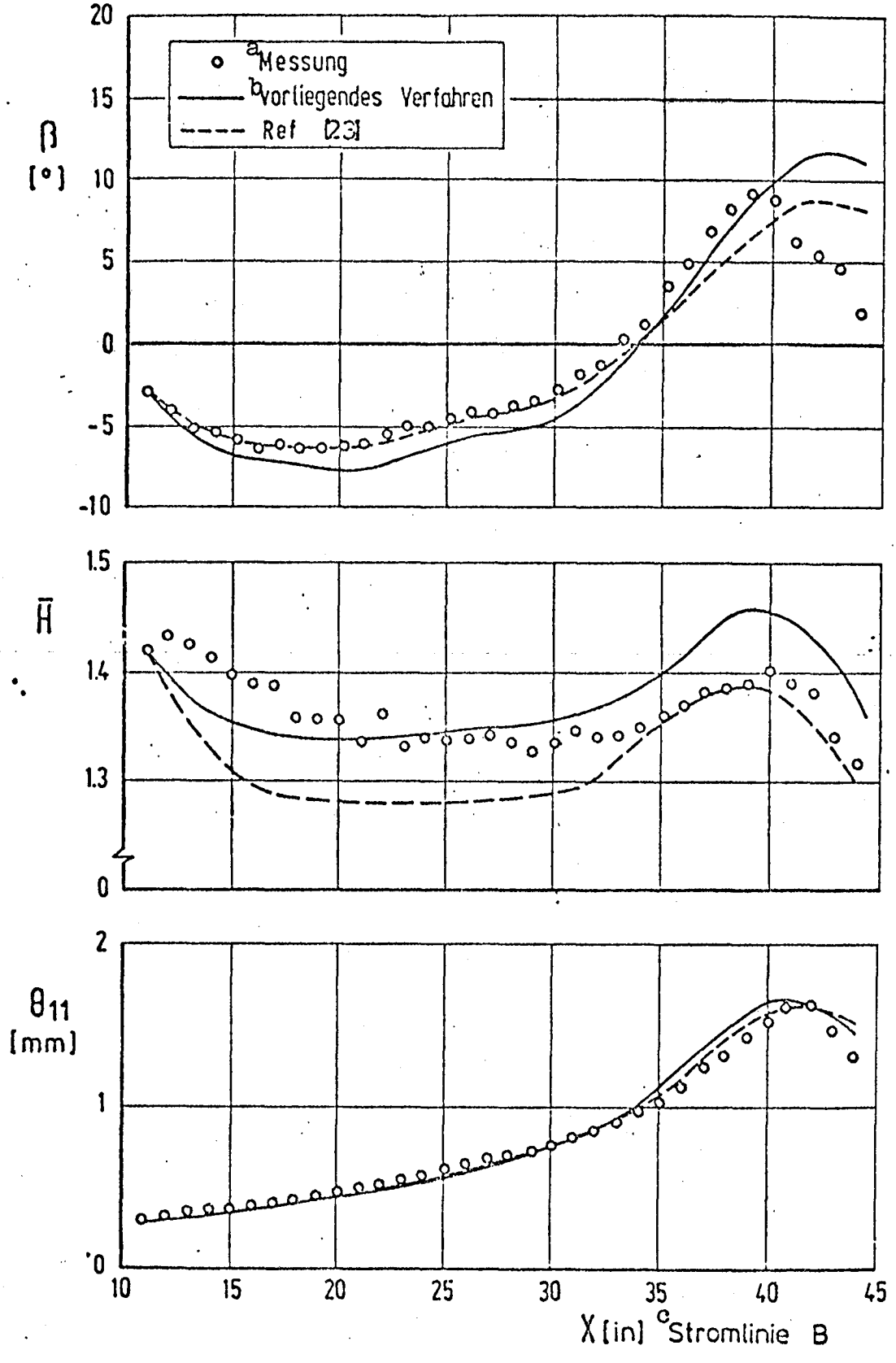

Fig. 11: Comparison of the calculated values of β, $\bar{H}$ and θ_{11} with measurements [22].

Key: a. measurement
b. present procedure
c. streamline

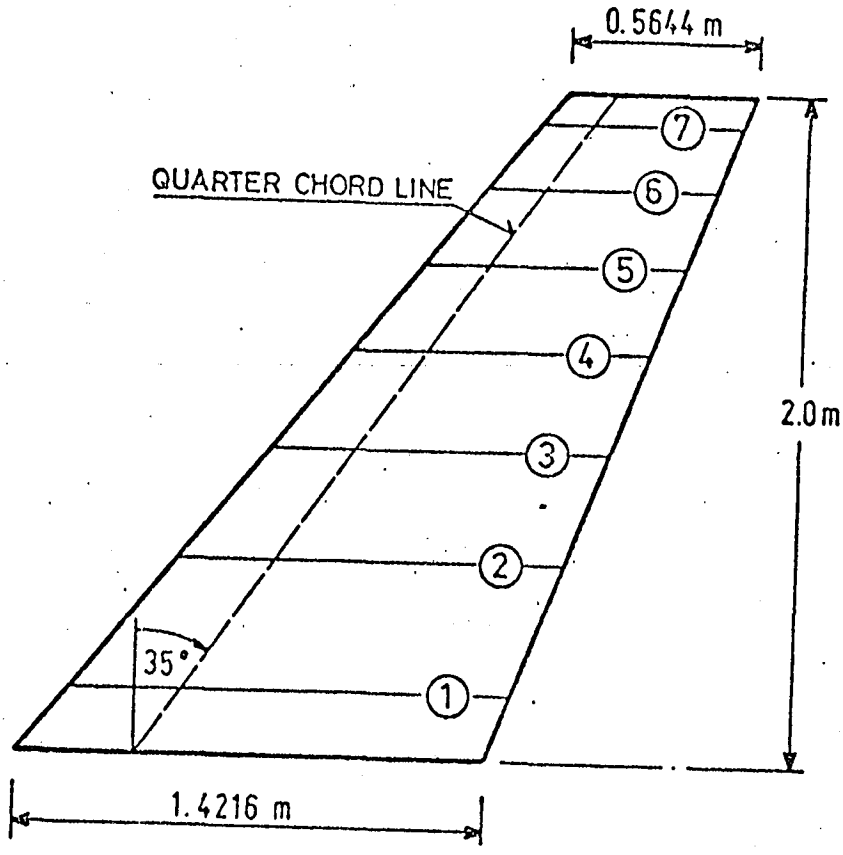

Fig. 12: Basic shape of the test wing (Eurovisc 1978).

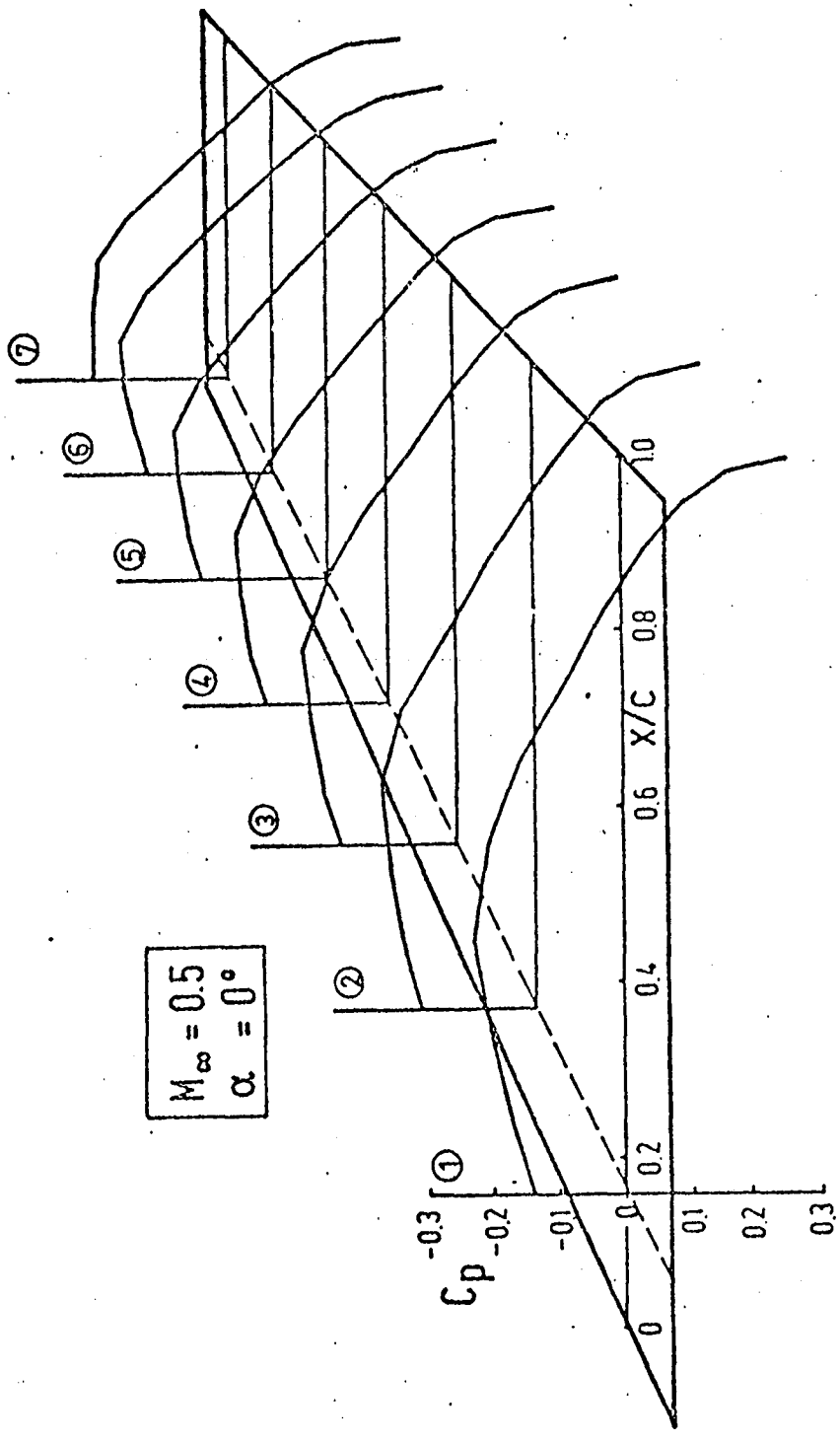

Fig. 13: Pressure distribution at the angle of inclination $\alpha = 0^0$

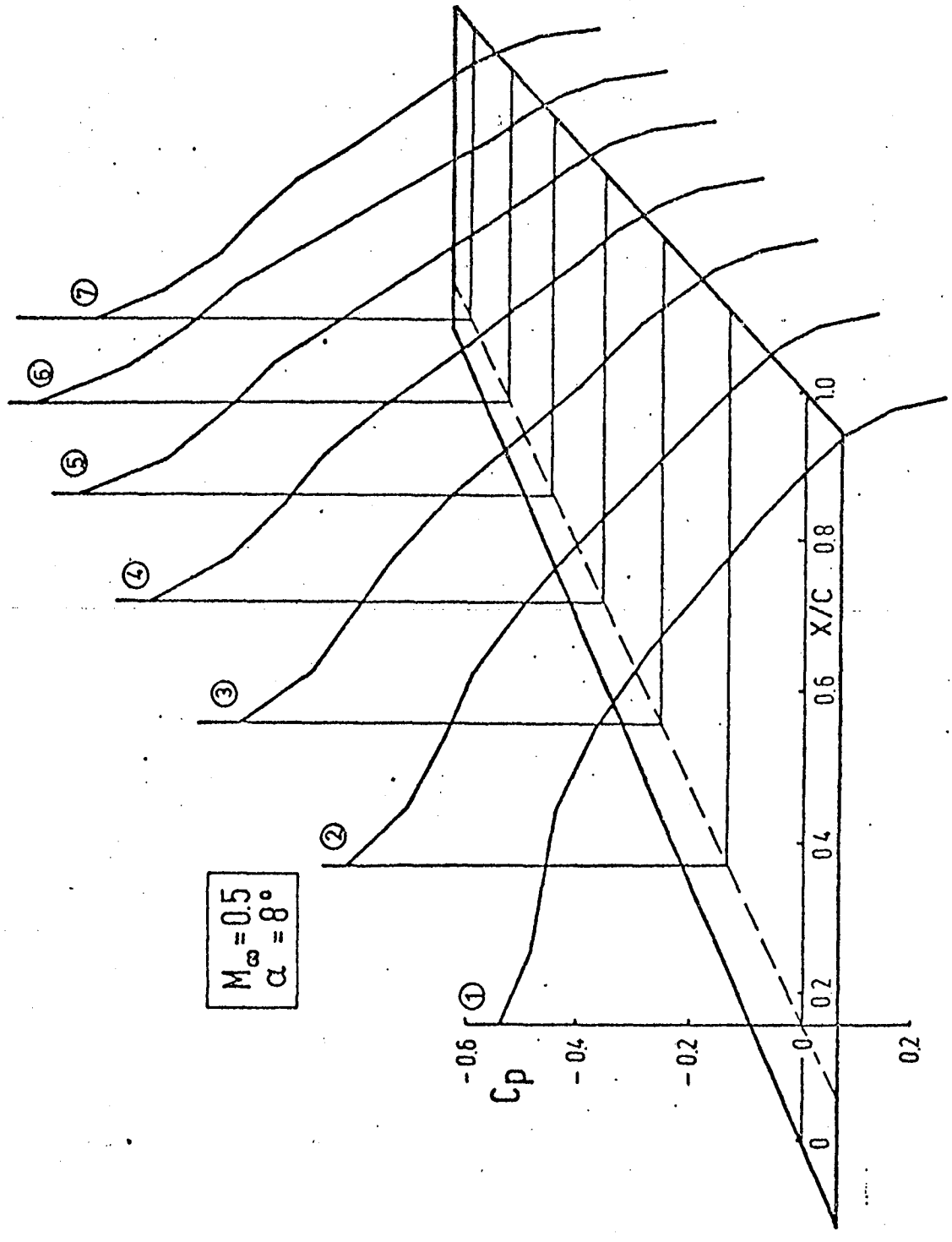

Fig. 14: Pressure distribution at an angle of inclination $\alpha = 8^0$

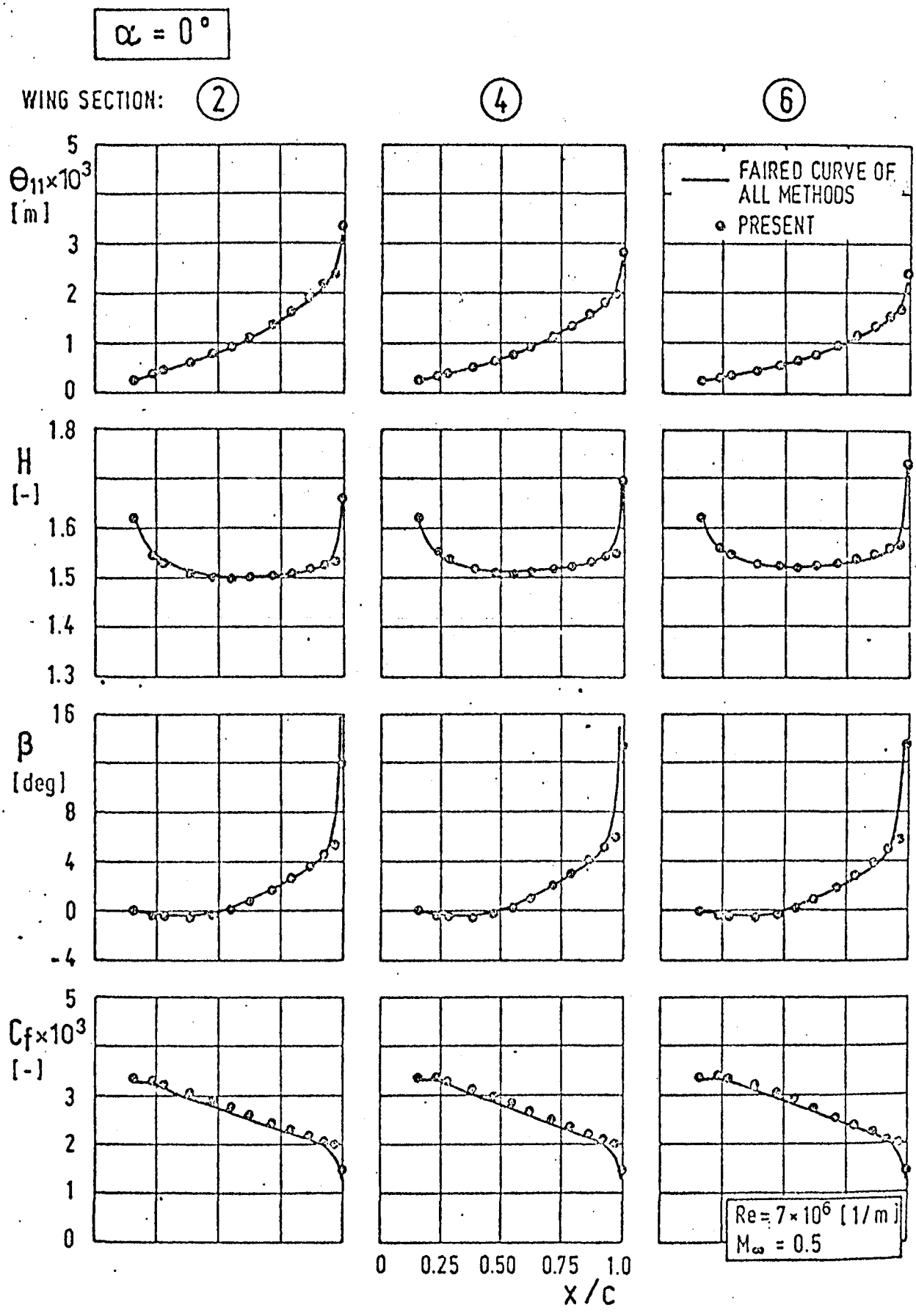

Fig. 15: Comparison of the calculated quantities θ_{11}, H, β and c_f with averaged results of the available calculations at $\alpha = 0^0$

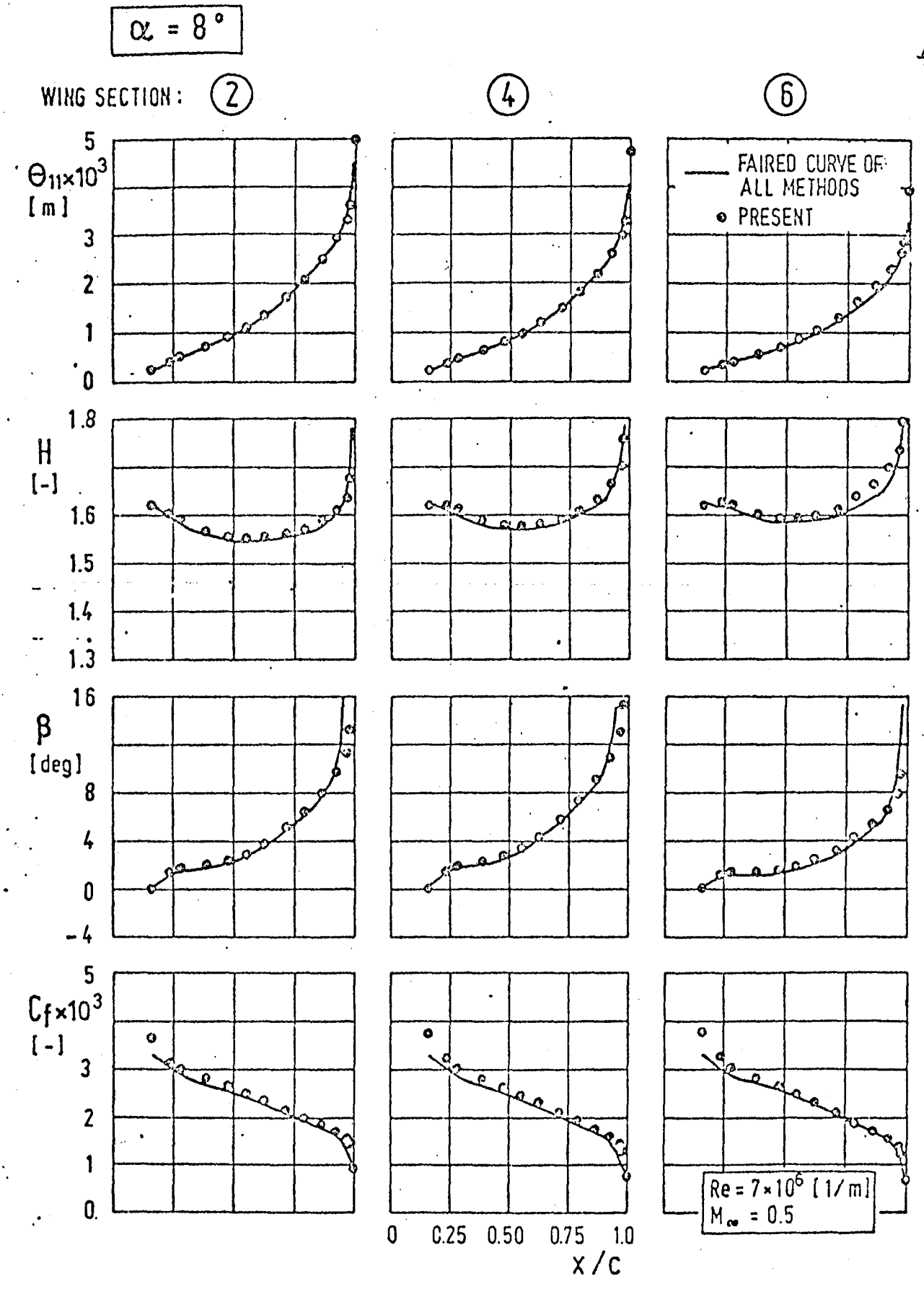

Fig. 16: Comparison of calculated quantities ϑ_{11}, H, β, and c_f with the averaged results of the available calculations at $\alpha = 8^0$

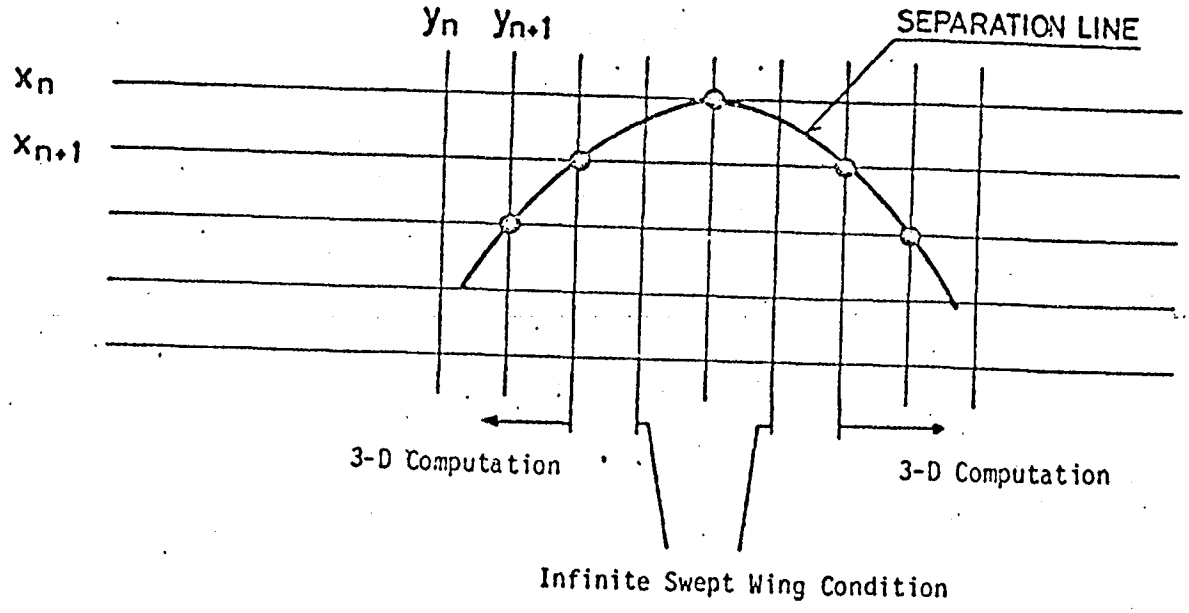

Fig. 17: Diagram for explaining the manner of calculation in the case of separated flow.

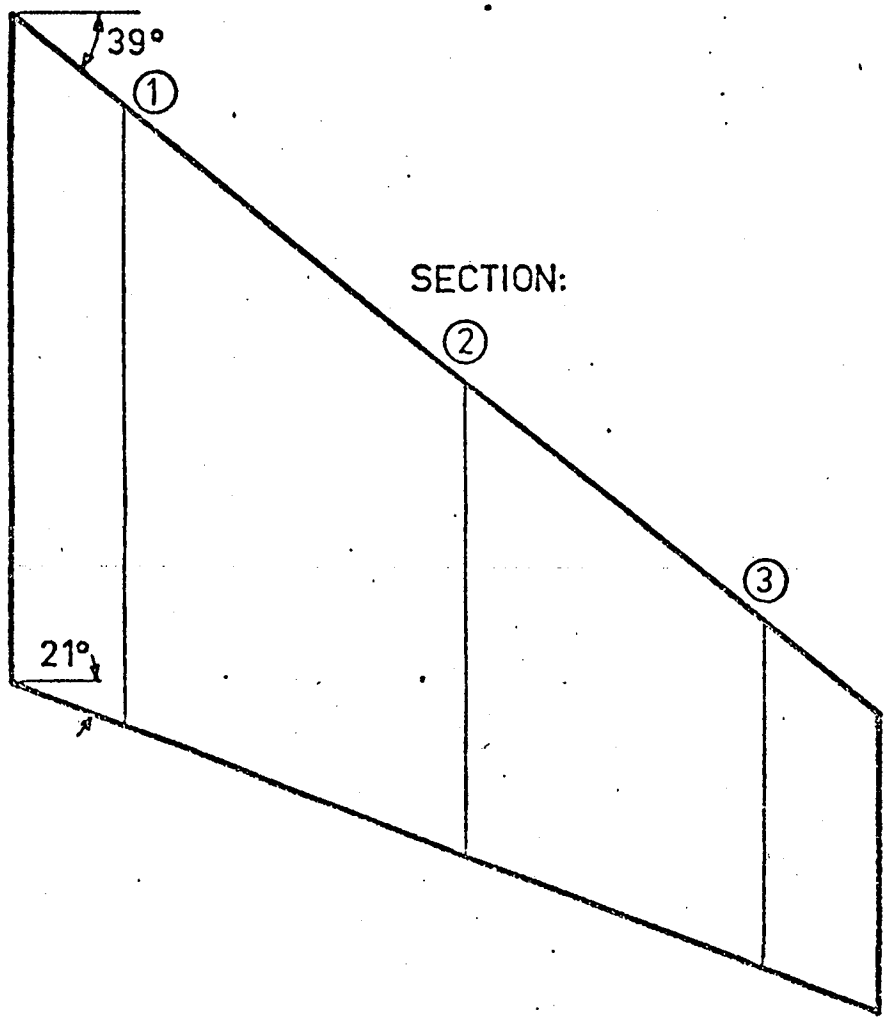

Fig. 18: Basic shape of the PT7.

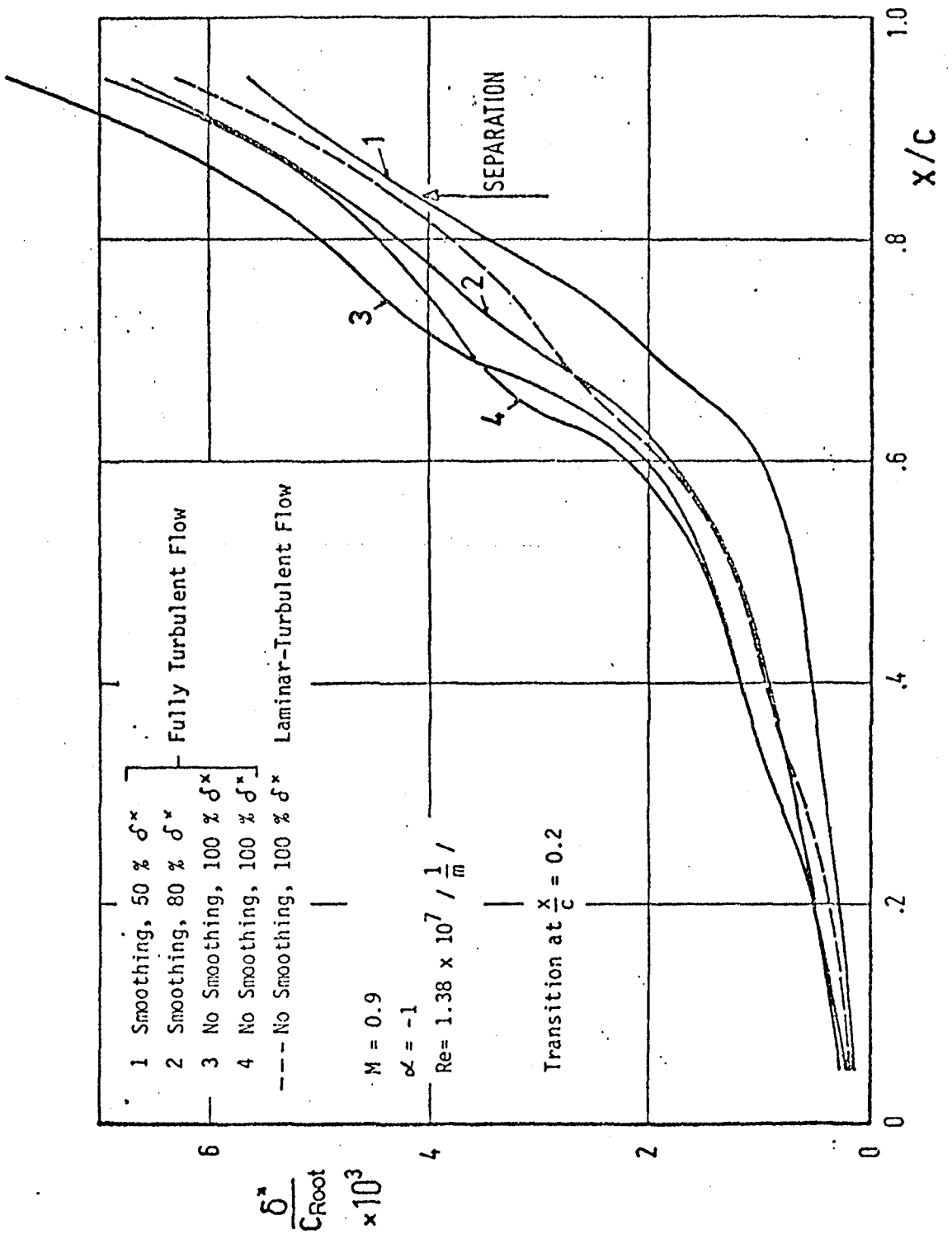

Fig. 19: Distribution of the displacement thickness on the upper side of the PT7 wing in the course of the iteration.

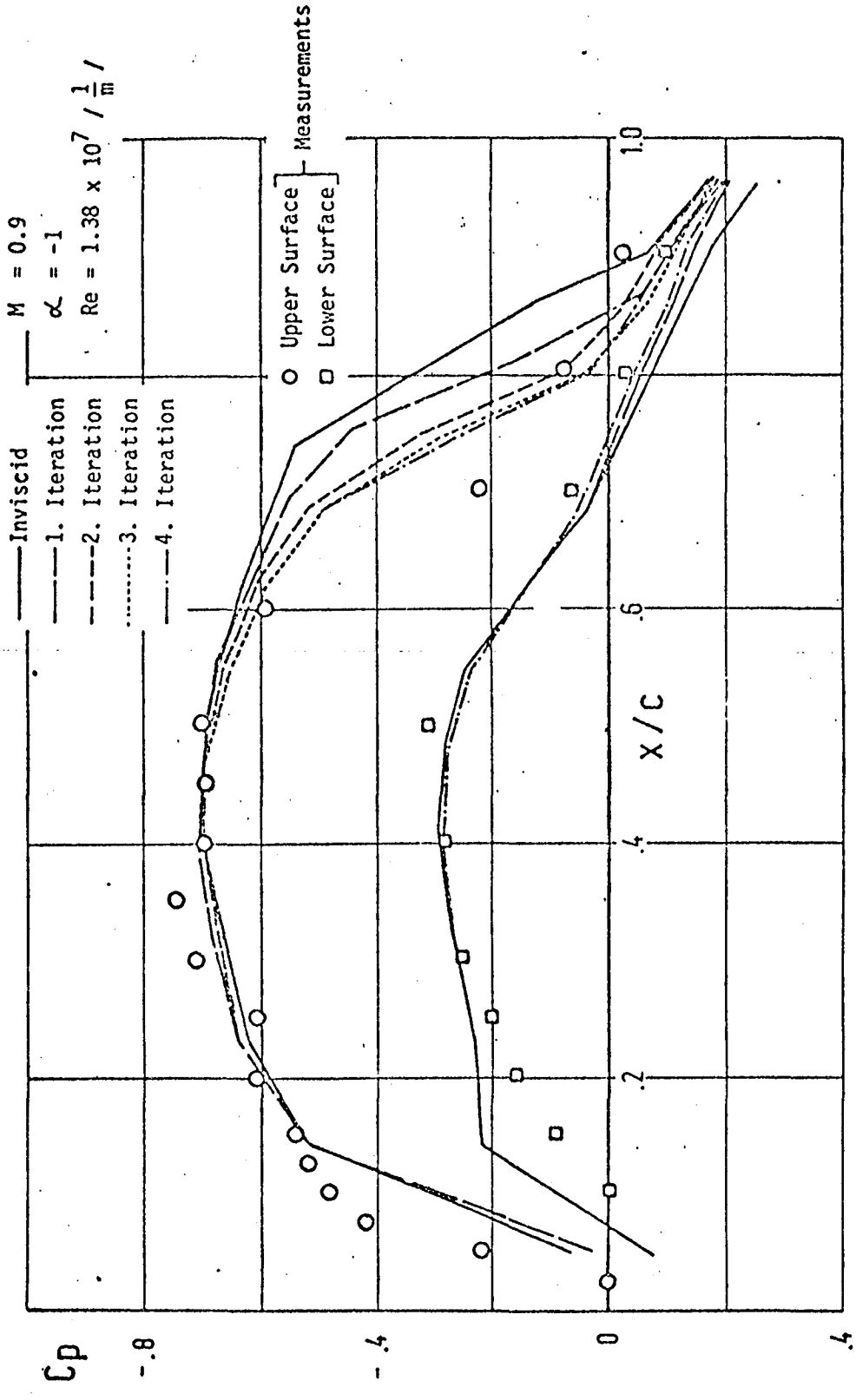

Fig. 20: Pressure distribution at the PT7 wing (section 1) in the course of the iterations and comparison with measurements.

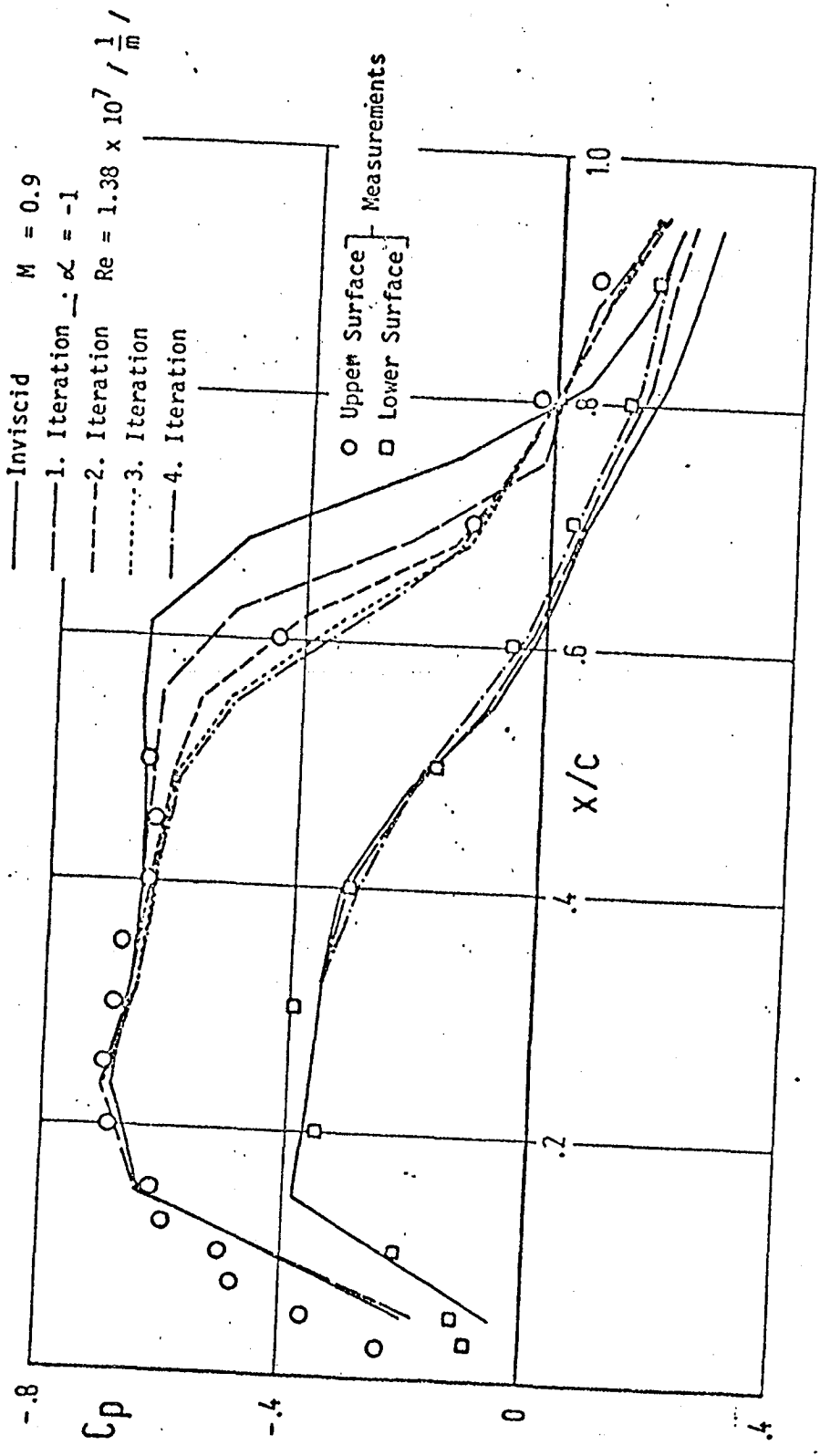

Fig. 21: Pressure distribution at the PT7 wing (section 2) in the course of the iterations and comparison with measurements.

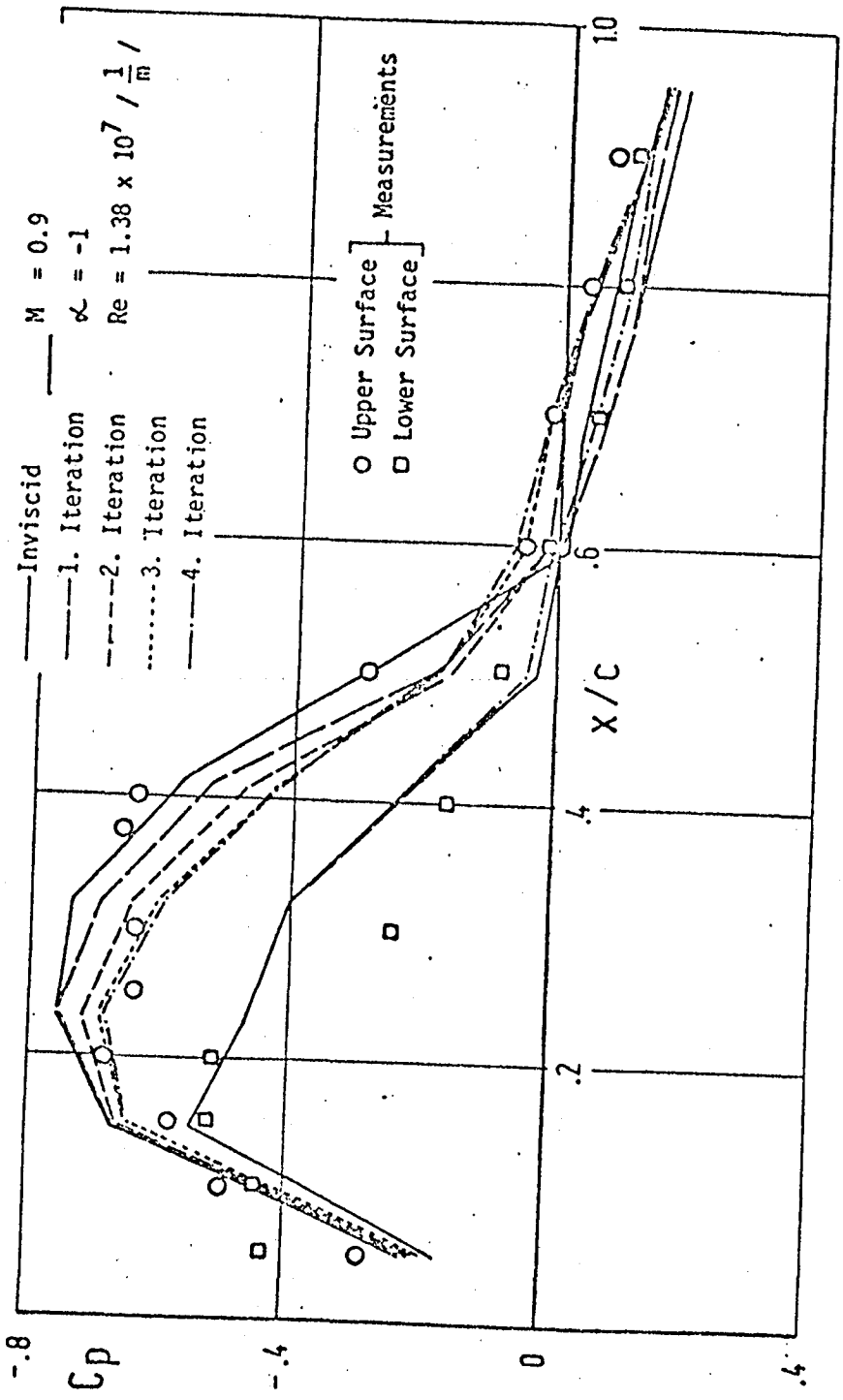

Fig. 22: Pressure distribution at the PT7 wing (section 3) in the course of the iterations and comparison with measurements.

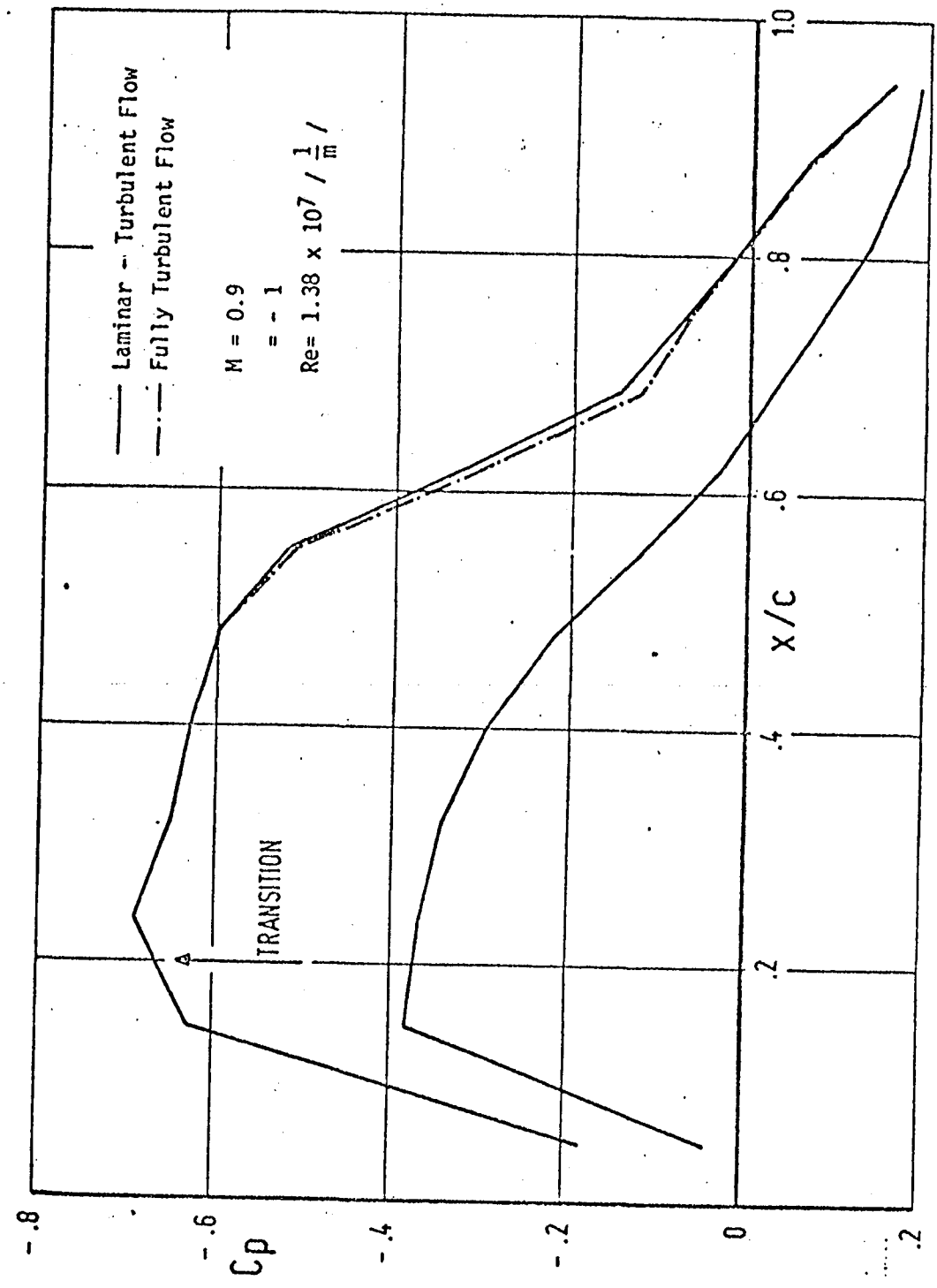

Fig. 23: Pressure distribution at the PT7 wing for fully turbulent and laminar turbulent flow (conversion at x/c = 0.2).

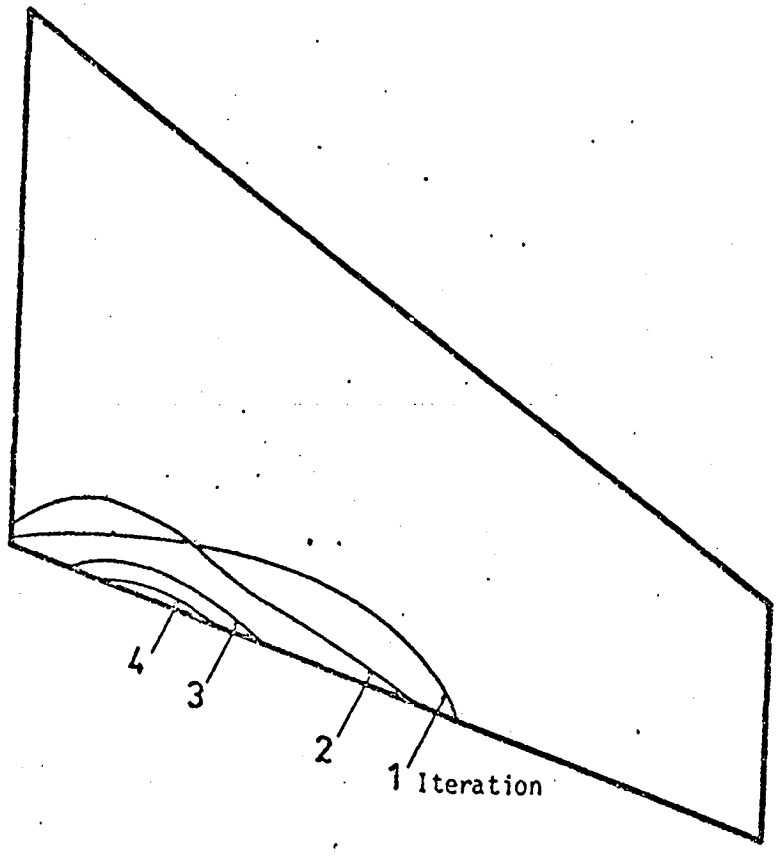

Fig. 24: Calculated separation lines in the course of the iterations.

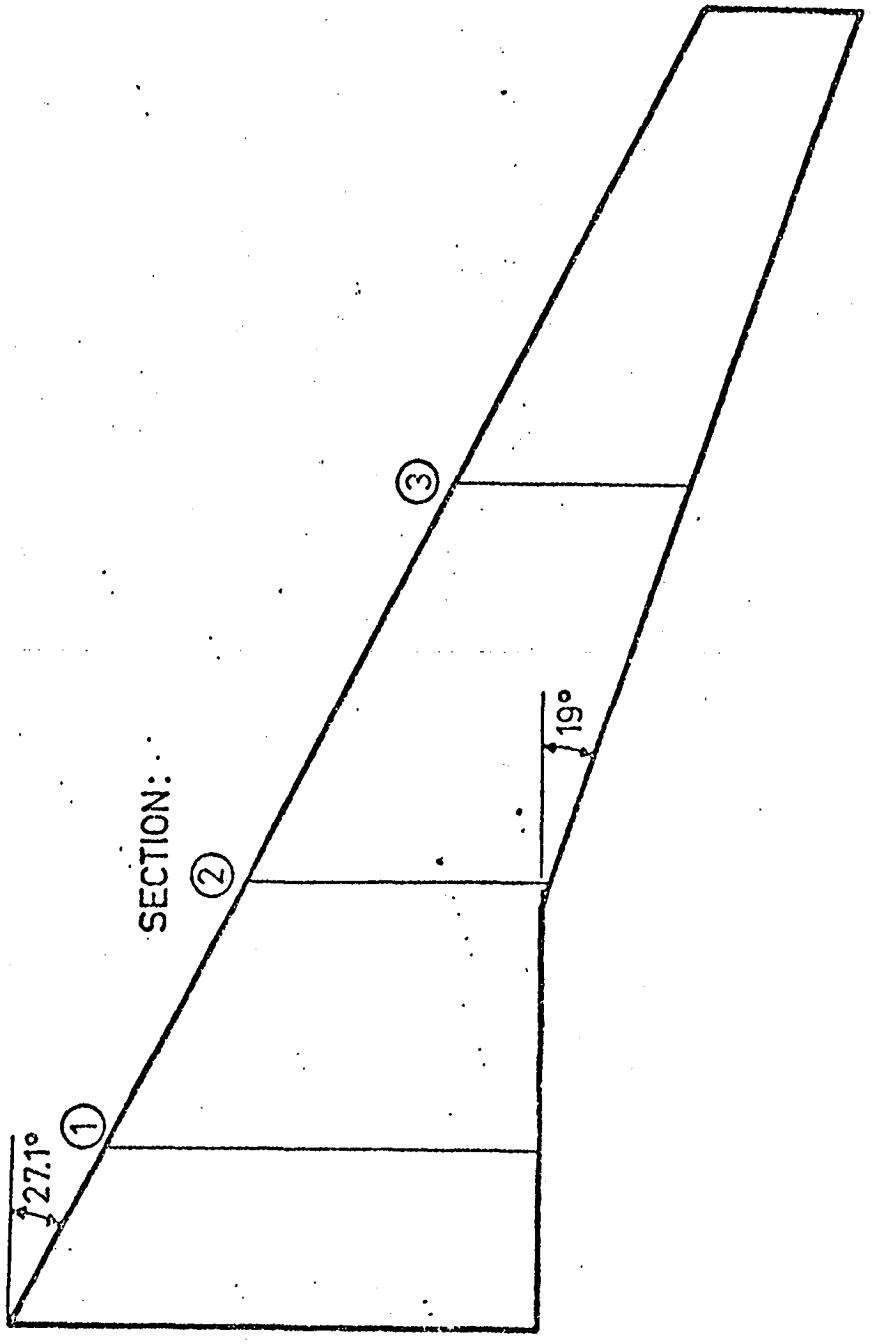

Fig. 25: Basic shape of the ZKP wing.

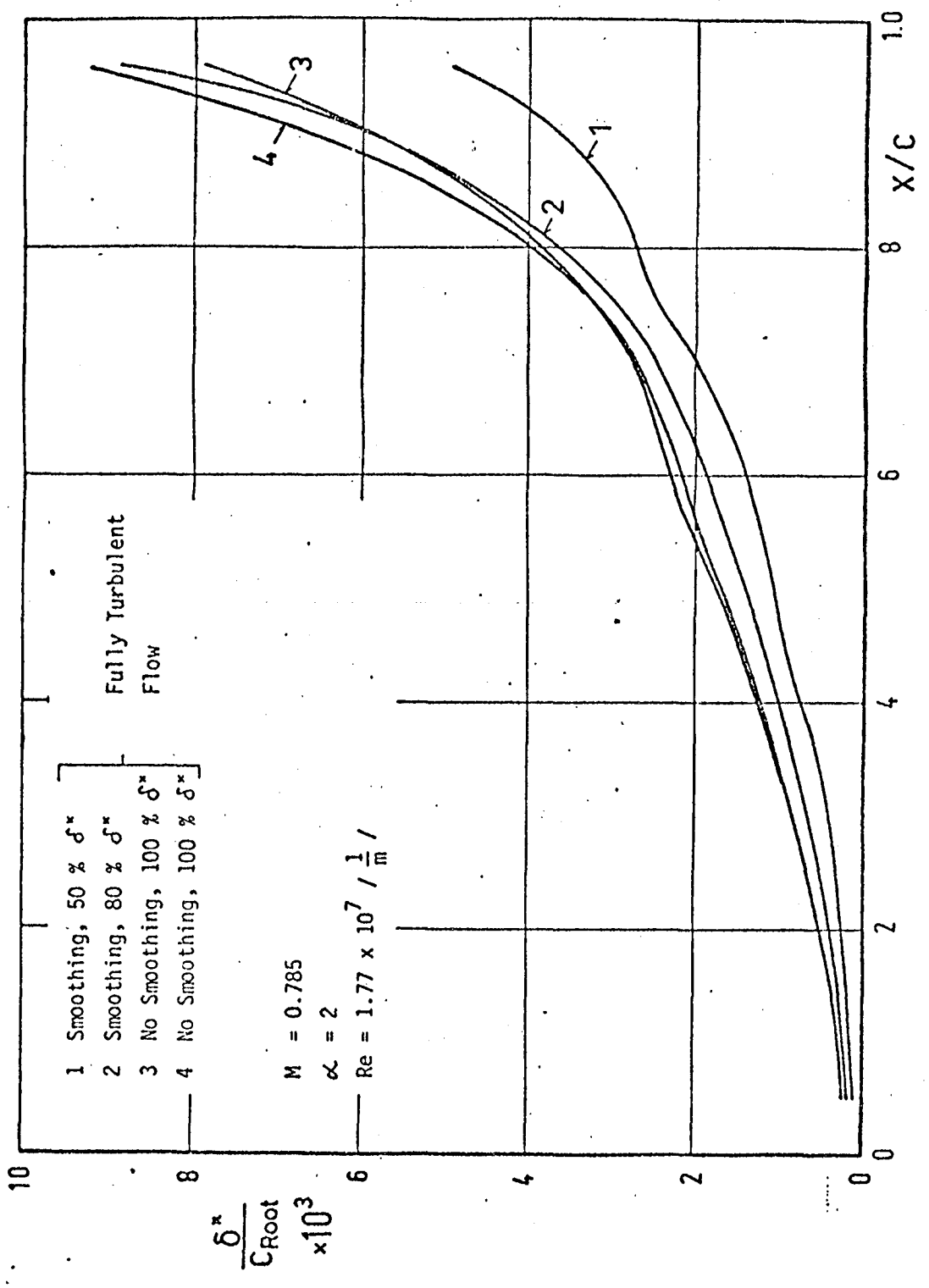

Fig. 26: Distribution of the displacement thickness at the ZKP wing (section 2) in the course of the iterations.

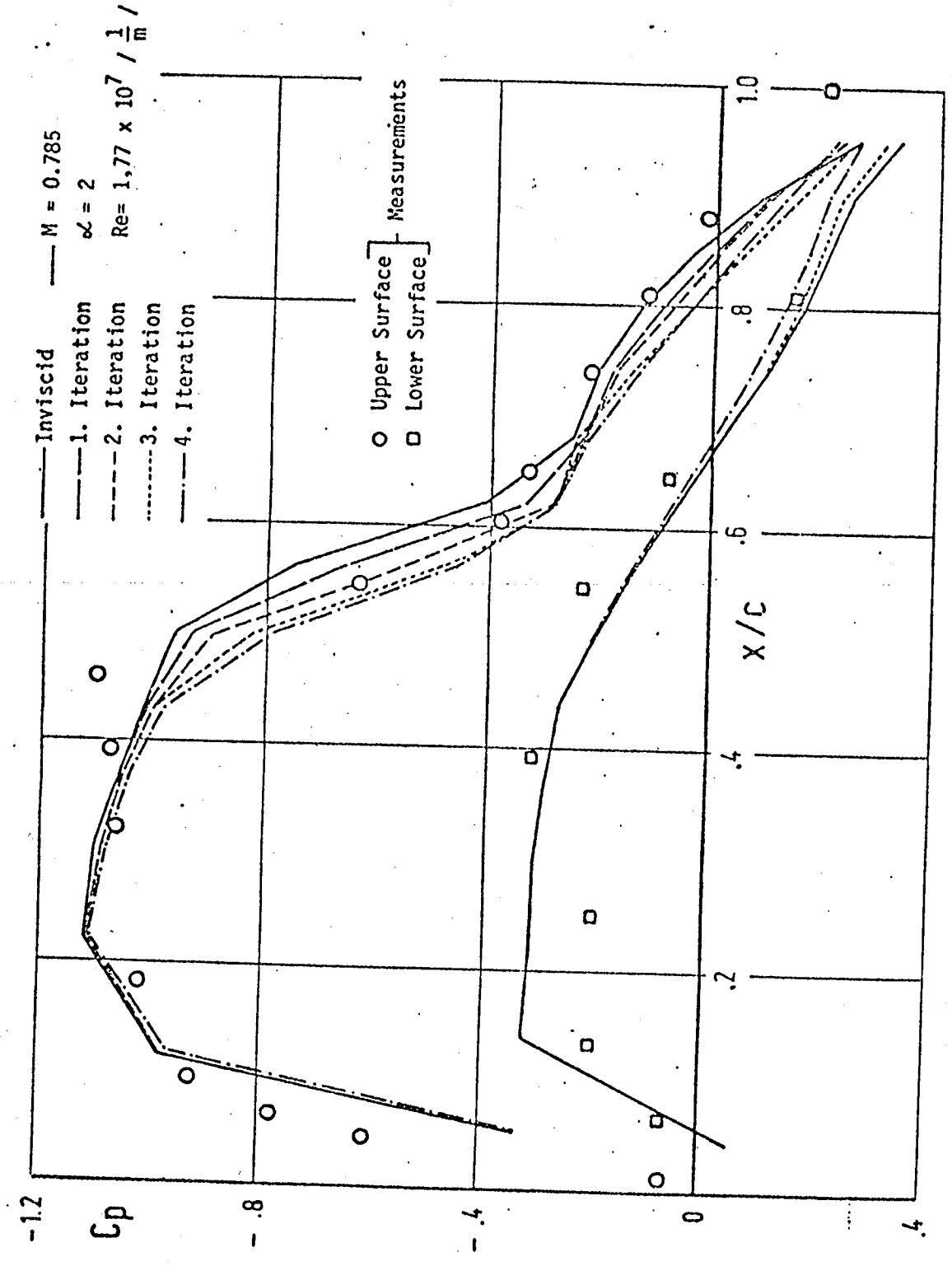

Fig. 27: Pressure distribution at the ZKP wing (section 1) in the course of the iterations and comparison with measurements.

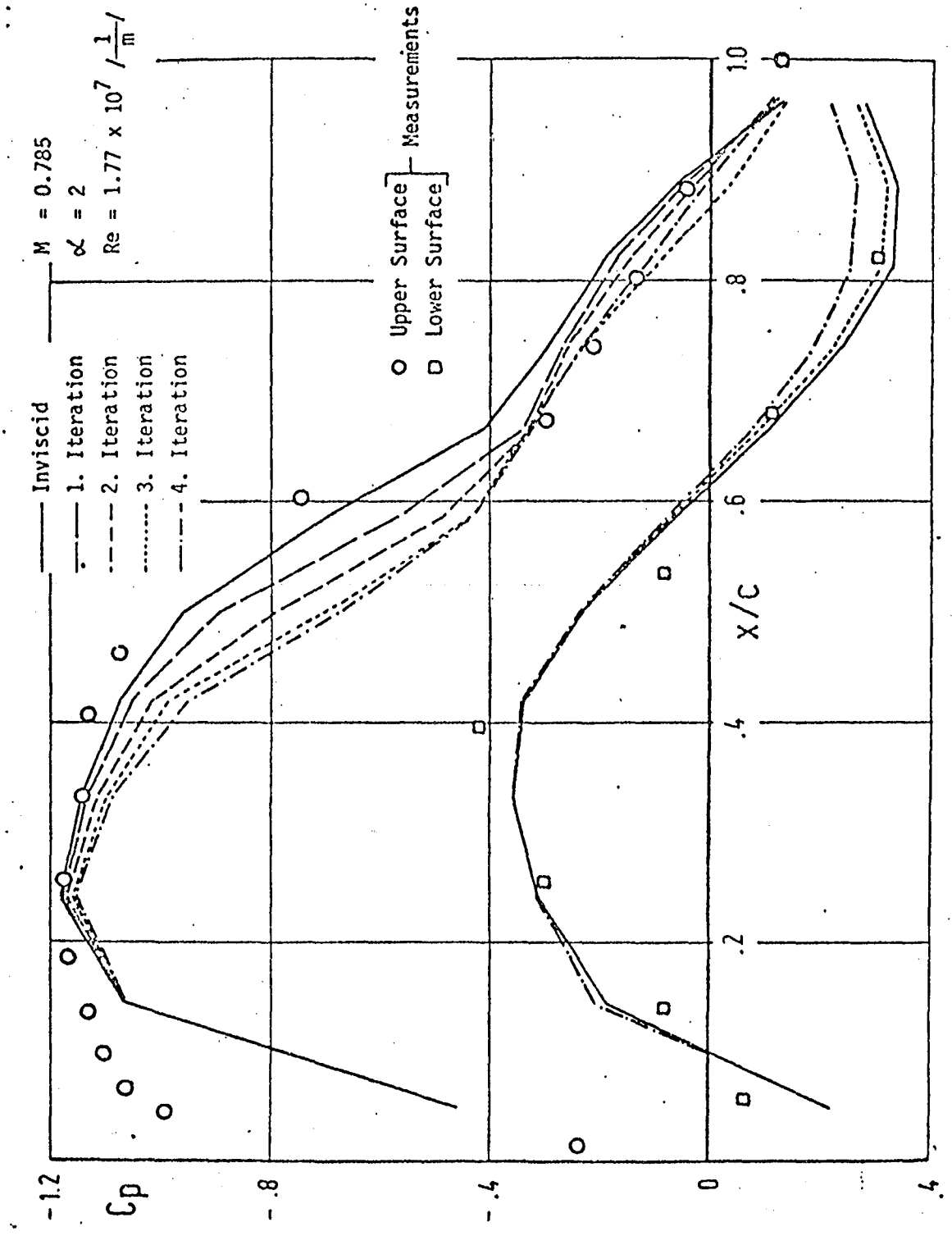

Fig. 28: Pressure at the ZKP wing (section 2) in the course of the iterations and comparison with measurements.

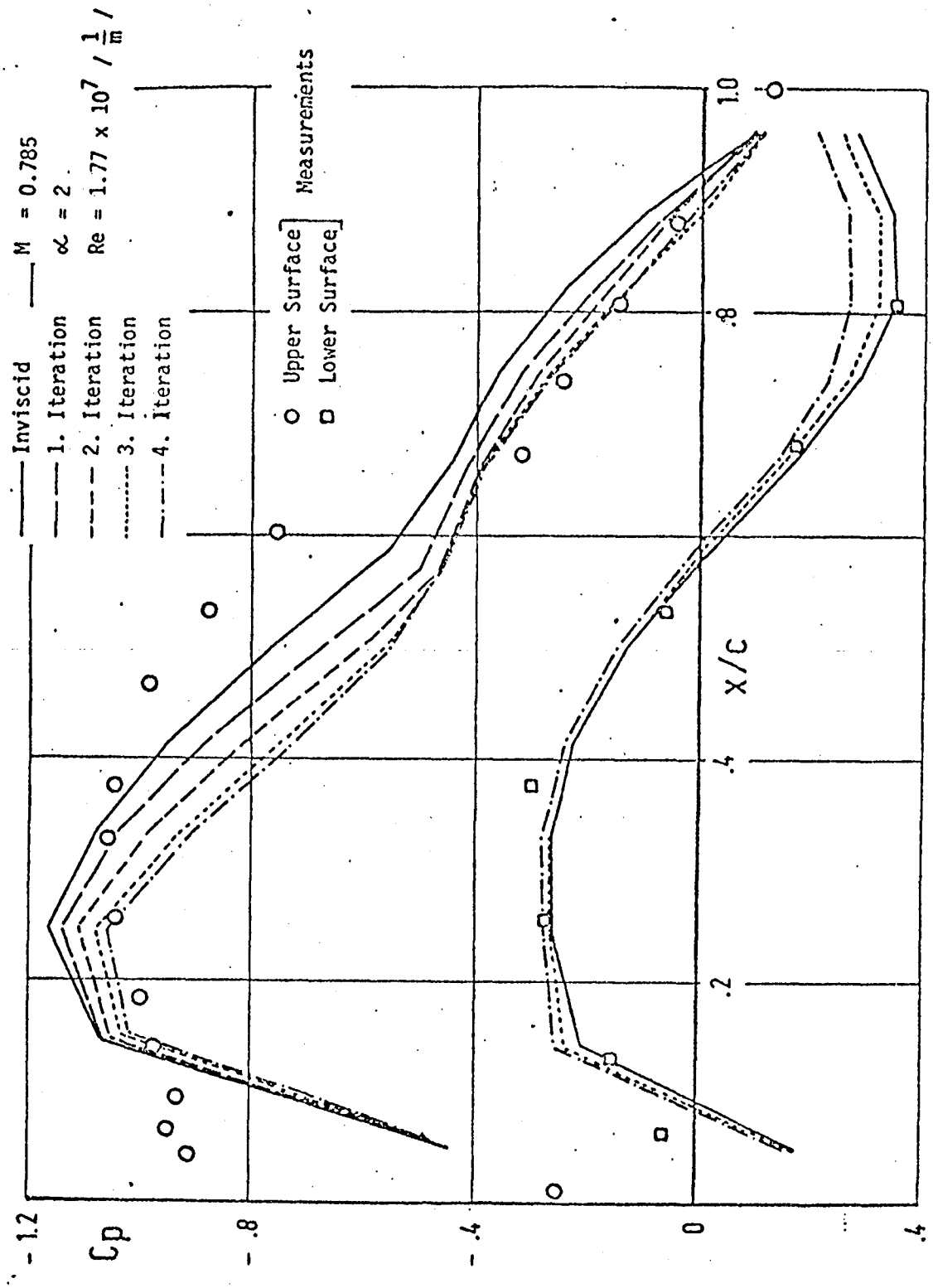

Fig. 29: Pressure distribution at the ZKP wing (section 3) in the course of the iterations and comparison with measurements.

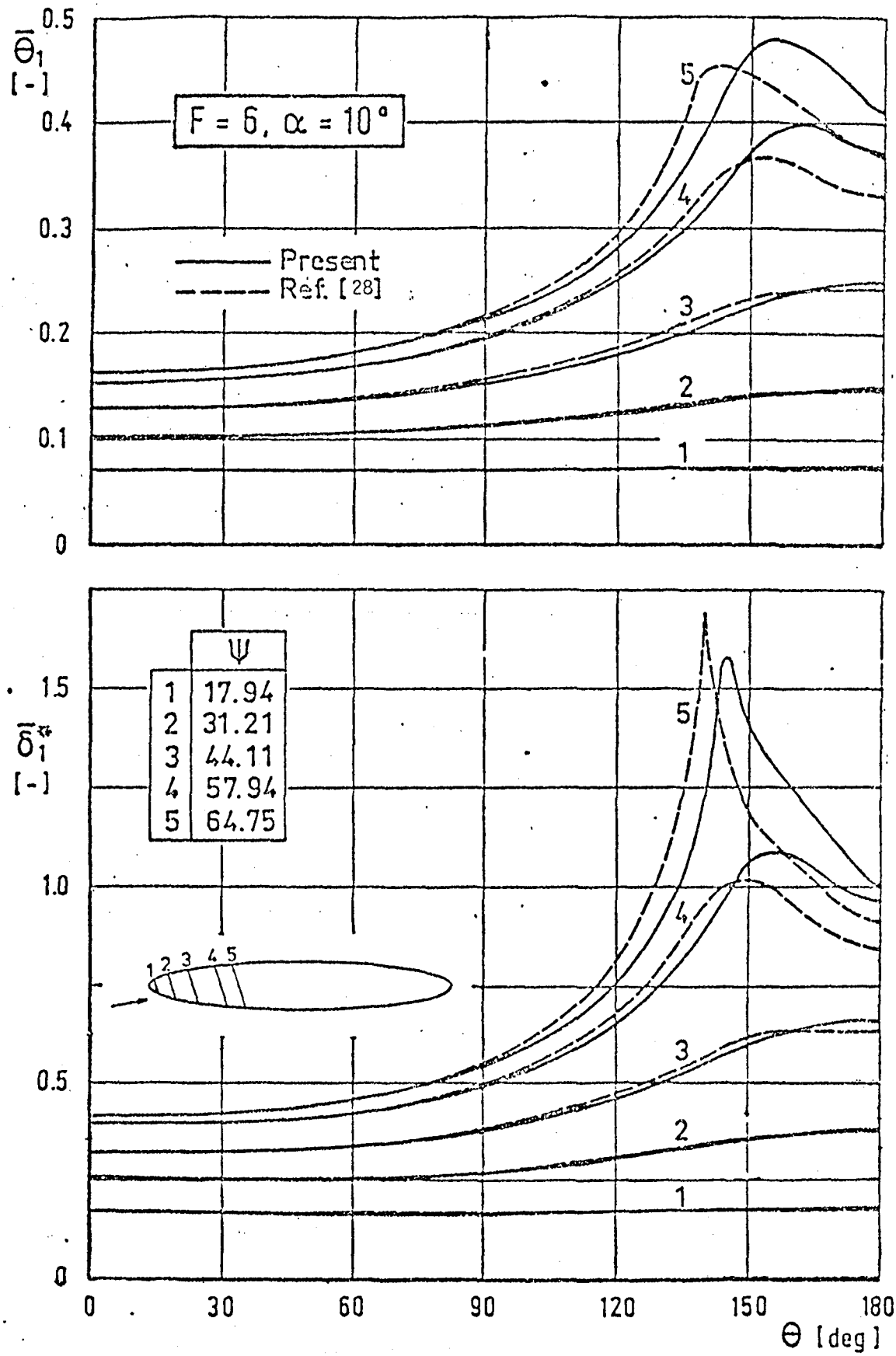

Fig. 30: Comparison of the $\bar{\theta}_1, \bar{\delta}_1^*, \bar{\tau}_w$ and ß with a difference procedure.

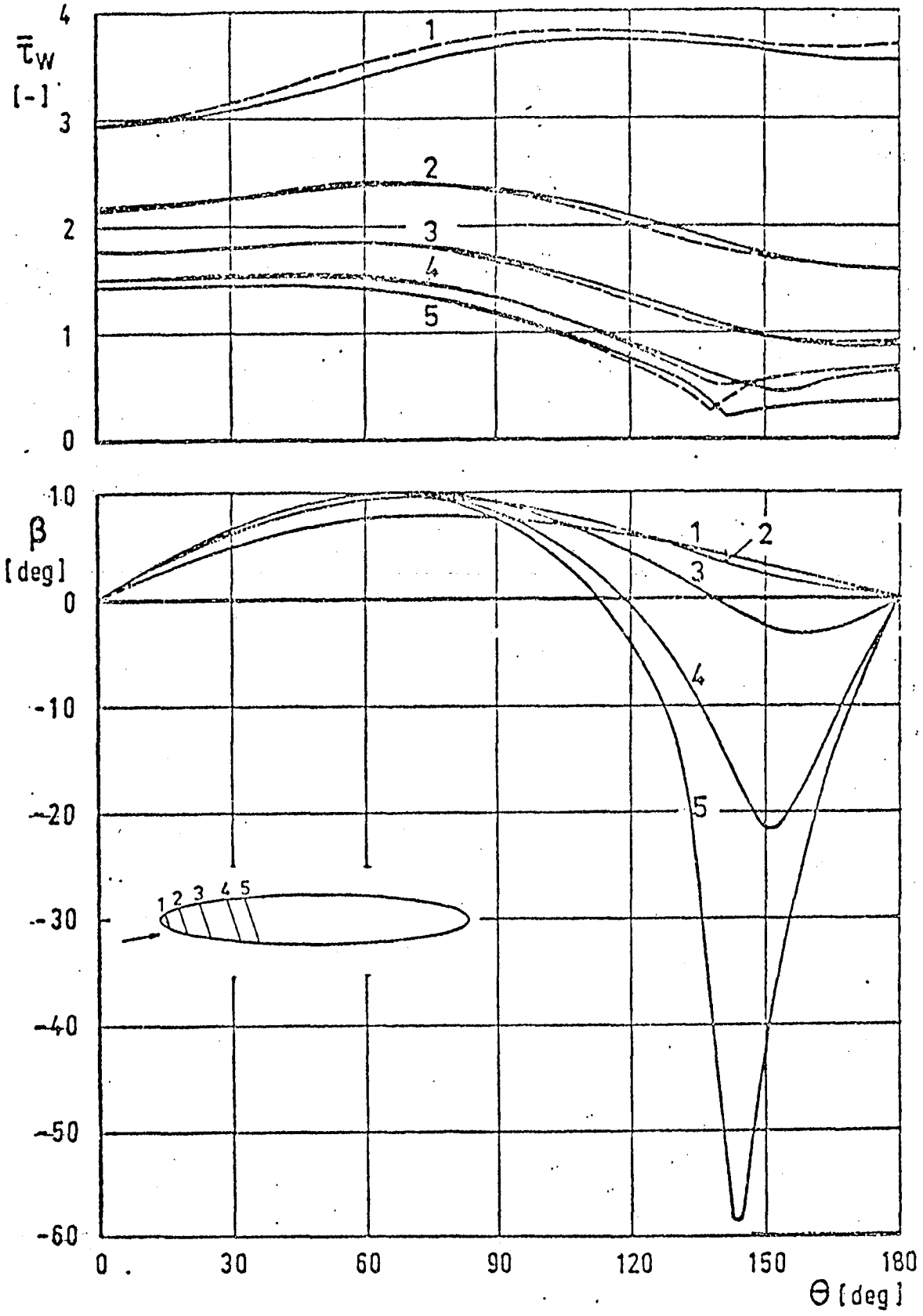

Fig. 30: continuation

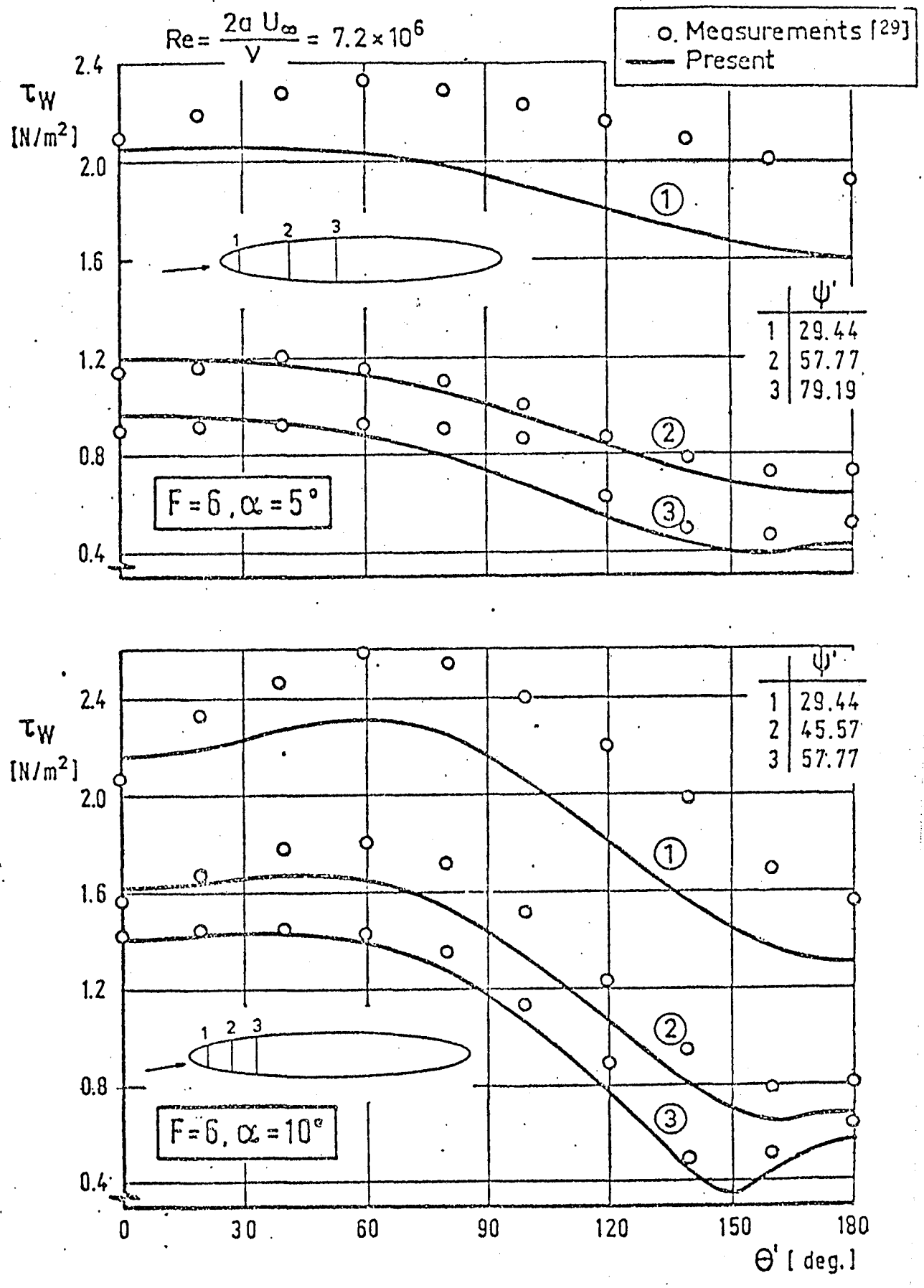

/79

Fig. 31: Comparison of the calculated surface shearing force τ_w with measurements [29].

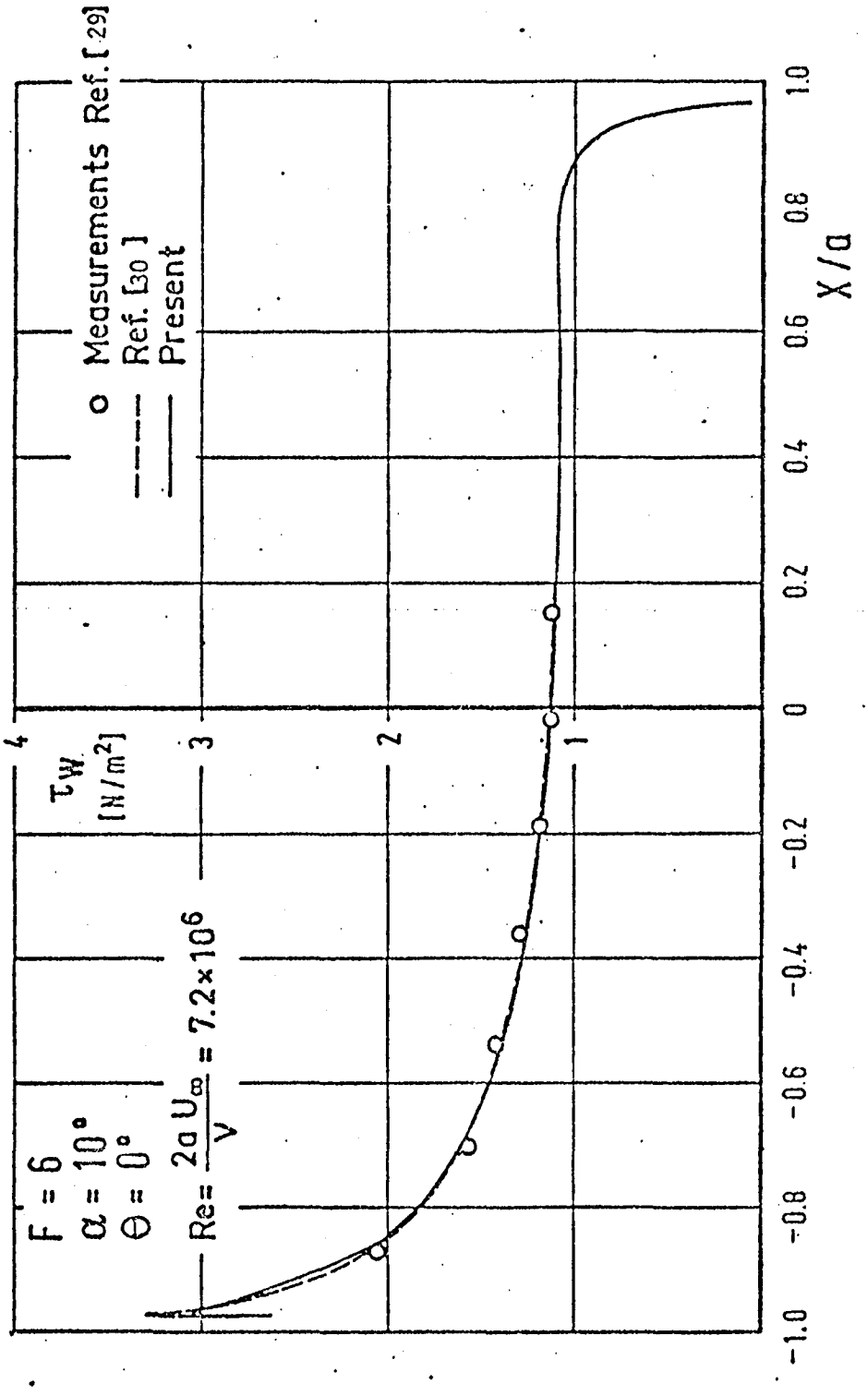

Fig. 32: Comparison of the calculated surface shearing force τ_w on the line of symmetry facing the wind with measurements[29].

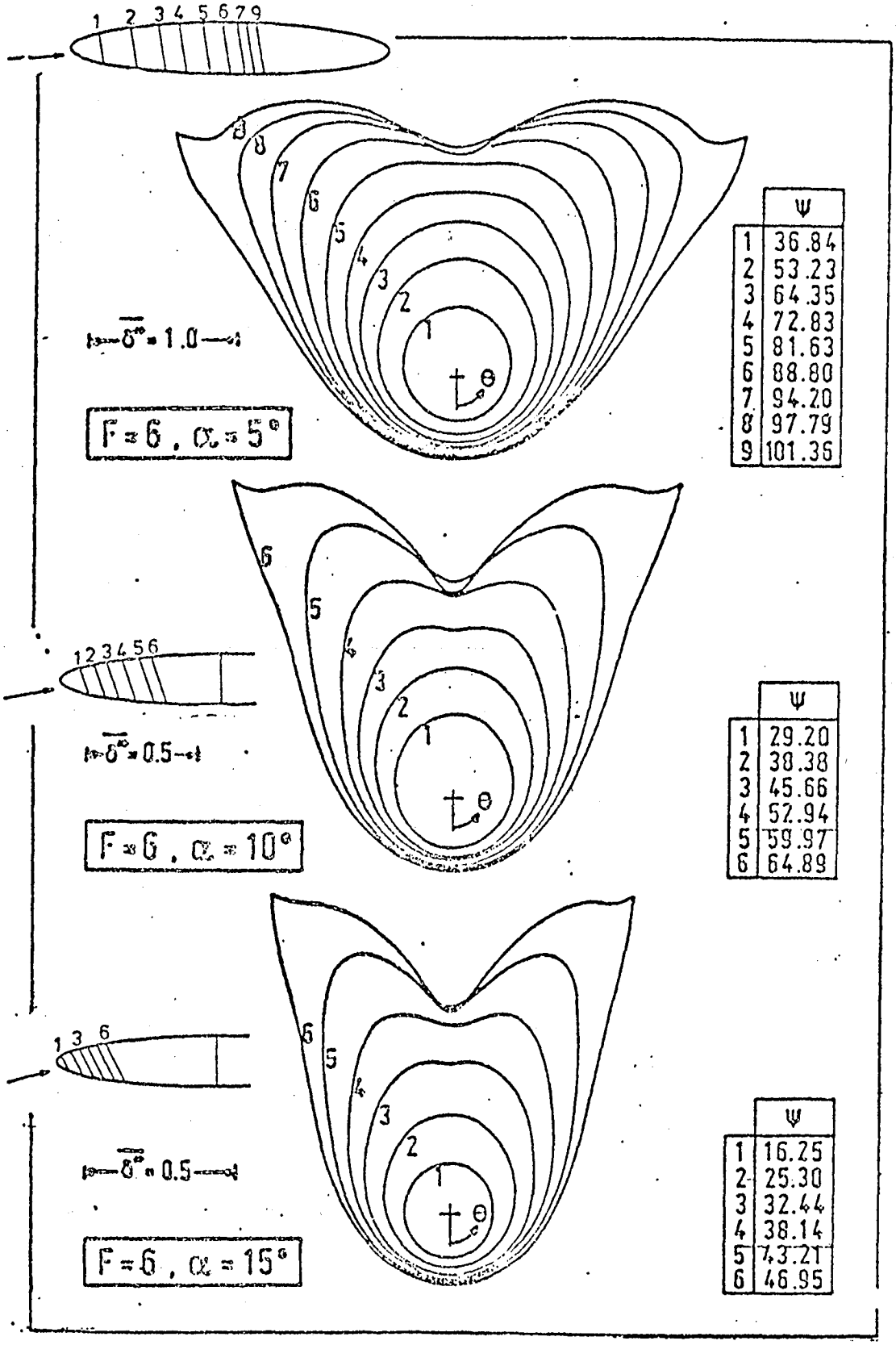

Fig. 33: The surface displacement distribution of an ellipsoid with a side ratio of 6:1.

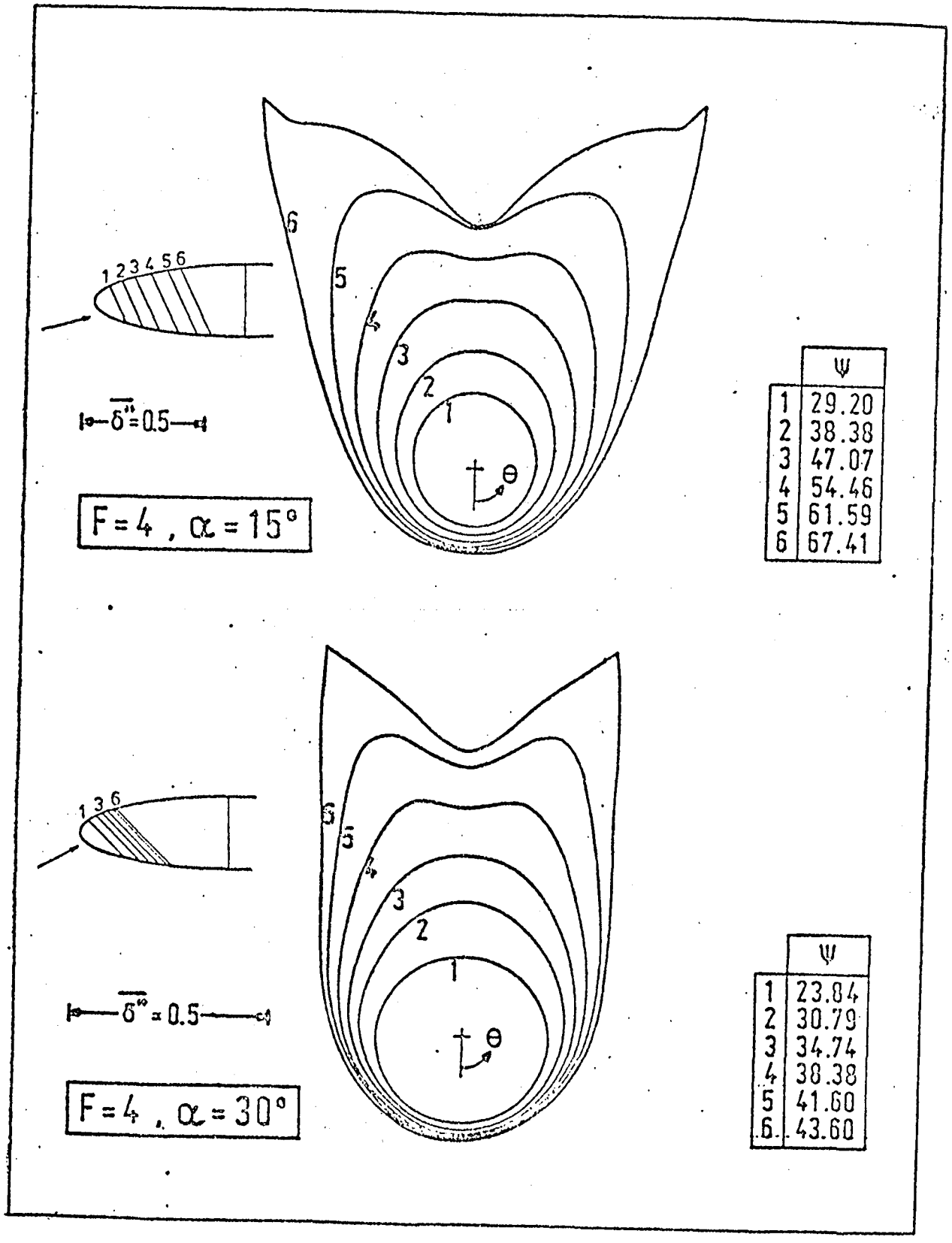

Fig. 34: The surface displacement distribution for an ellipsoid with a side ratio of 4:1.

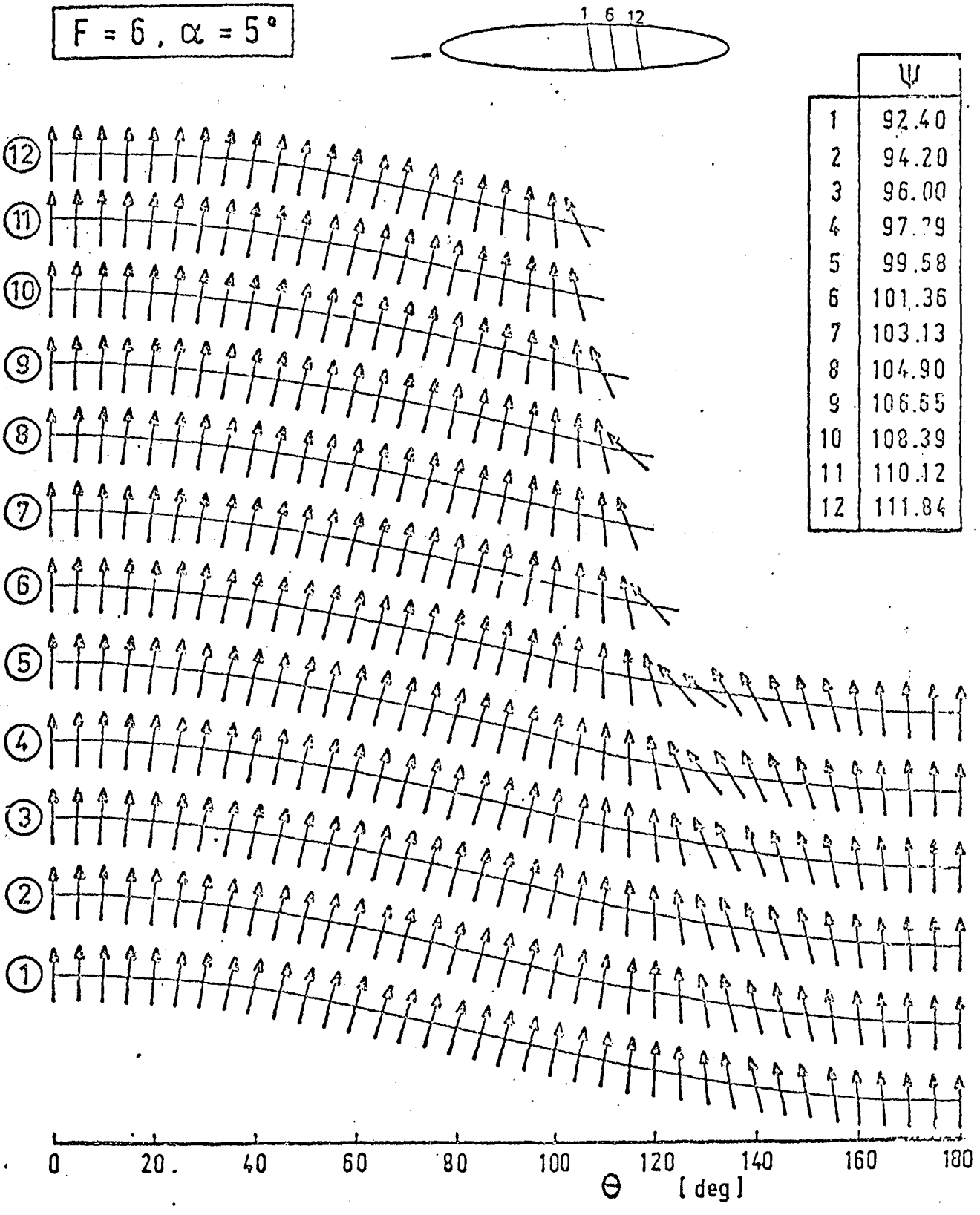

Fig. 35: Illustration of the direction of the resulting surface shearing force.

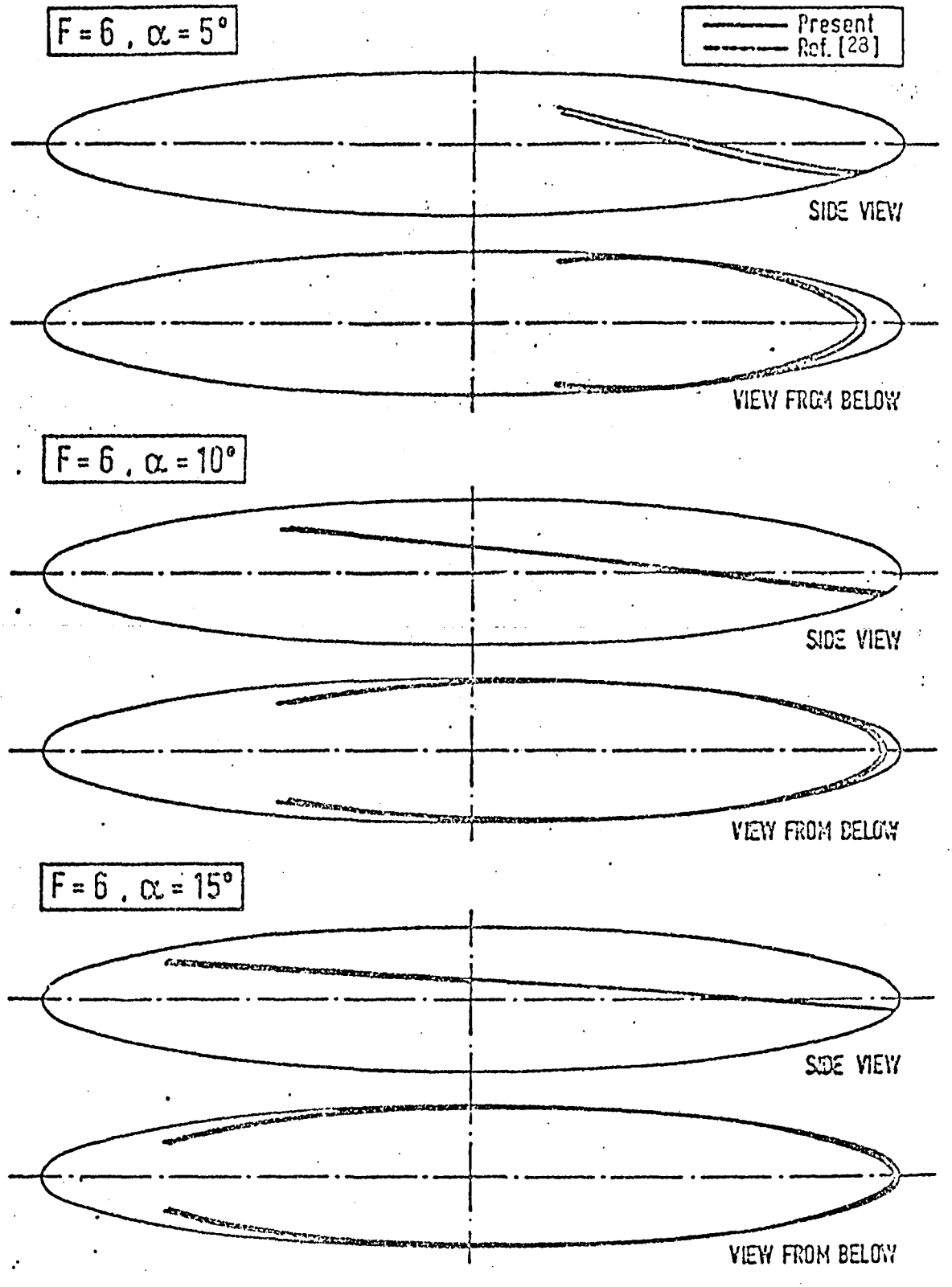

Fig. 36: Comparison of the turbulence departure lines for the ellipsoid with a side ratio of 6:1.

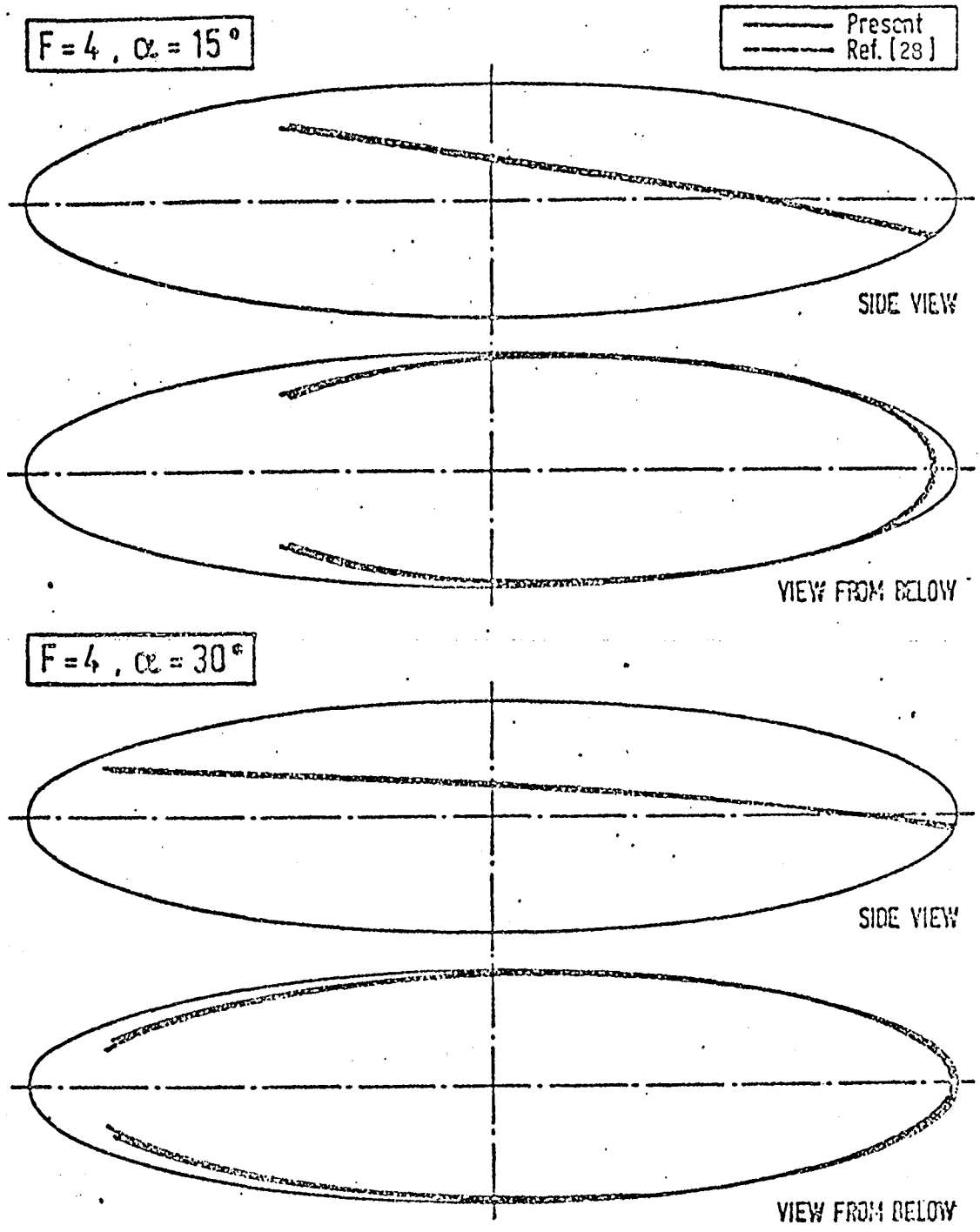

Fig. 37: Comparison of the turbulence departure lines for the ellipsoid with a side ratio of 4:1.

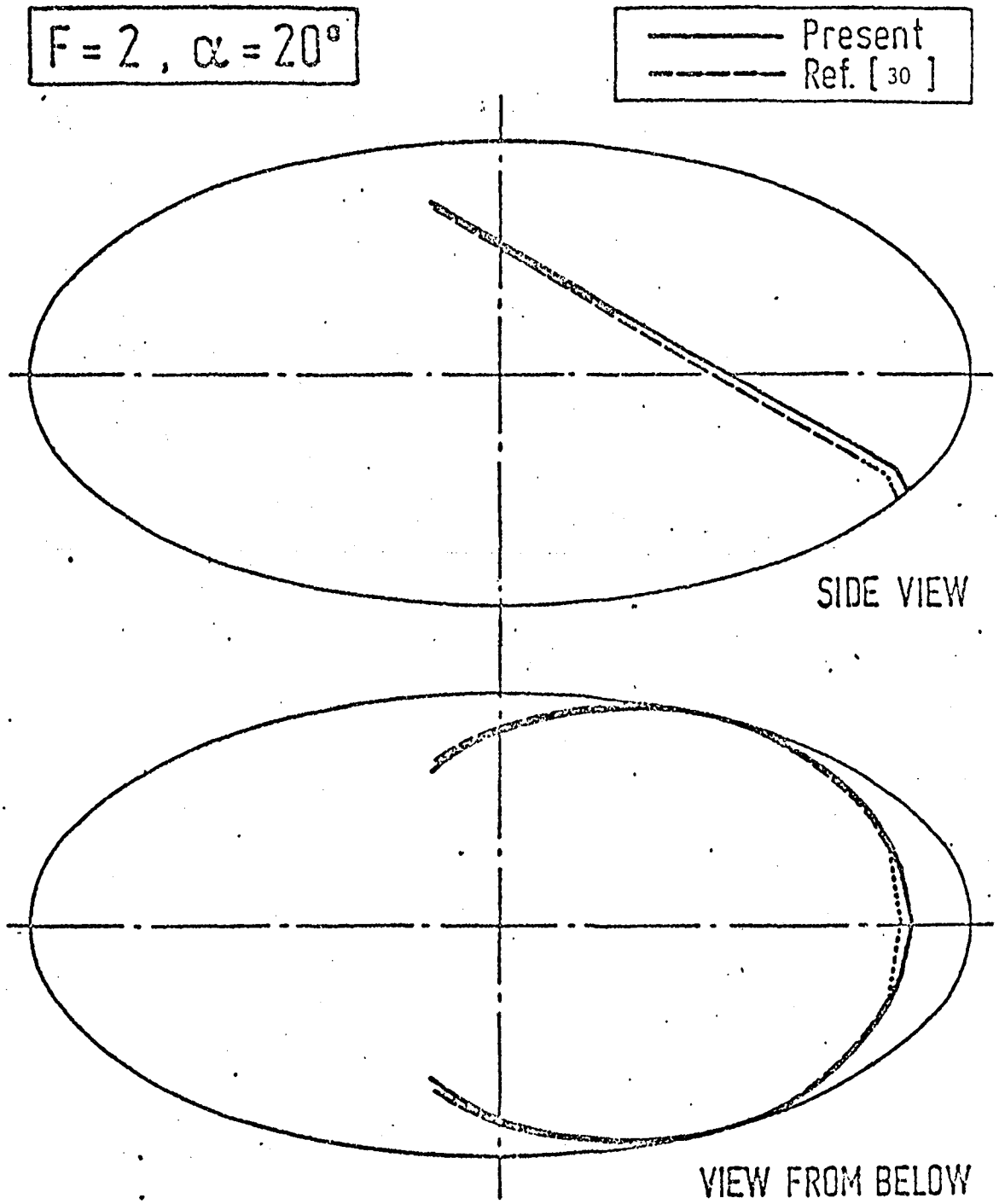

Fig. 38: Comparison of the turbulence departure lines for the ellipsoid with the side ratio of 2:1.

REFERENCES

[1] Goldstein, S., "On laminar boundary layer flow near a position of separation", Quart. J. Med. Appl. Meth., 1, p. 43-69 (1948).

[2] Brown, S. N. and K. Stewartson, "Laminar Separation", Annual Review of Fluid Mechanics, Annual Reviews Inc., p. 45-72 (1969).

[3] Catherall, D. and K. W. Mangler, "The Integration of Two-Dimensional Laminar Boundary Layer Equations Past the Point of Vanishing Skin Friction", J. Fluid. Mech., Vol. 26, p. 163-182 (1966).

[4] Kuhn, G. D. and J. N. Nielsen, "Prediction of Turbulent Separated Boundary Layers", AIAA J. Vol. 12, no. 7, p. 881-882 (1974).

[5] Bower, W. W., "Analytical Procedure for Calculation of Attached and Separated Subsonic Diffuser Flow", AIAA J. Vol. 13, no. 1, p. 49-56 (1976).

[6] Assassa, G. M. and B. Gay, "Prédiction numérique des éconlements turbulents au voisinage du point de décollement", Entropie, Vol. 14, p. 29-38 (1978).

[7] East L. F., P. D. Smith and P. J. Merryman, "Prediction of the Development of separated Turbulent Boundary Layers by the Lag-Entrainment Method", RAE TN No. 77046, 1977.

[8] Le Balleur, J. C. and J. Mirande, "Etude Expérimentele et Théorique du Recollement Bidimensional Turbulent Incompressible", ONERA T. P. No. 1975, 16 (1975).

[9] Thiede, P., "Extension of the Boundary Layer Concept to the Calculation of Two-Dimensional Separated Flows", BMVg-FBWT 77-20, 1977.

[10] Carter, J. E., "Inverse Solutions for Laminar Boundary Layer Flows with Separation a nd Reattachment", NASA TR R-447, 1975.

[11] Cebeci, T., "An Inverse Boundary Layer Method for Compressible Laminar and Turbulent Boundary Layers", AIAA J. Vol. 13, No. 9, p. 709-717 (1976).

[12] Coles, D., "The Law of the Wake in the Turbulent Boundary Layer", J. Fluid. Mech. Vol. 1, Part 2, p. 191-226 (1956).

[13] Mager, A., "Generalisation of Boundary Layer Momentum Integral Equations to Three-Dimensional Flows, Including those of Rotating Systems", NACA Rep. 1067, 1952.

[14] Johnston, J. P., "On the Three-Dimensional Turbulent Boundary Layer Generated by Secondary Flow", J. of Basic Eng. Vol. 82, p. 223-250 (1960).

[15] Smith, P. D., "An Integral Prediction Method for Three-Dimensional Compressible Turbulent Boundary Layers", ARC, R&M No. 3739, 1979.

[16] Stock, H. W., "An Integral Method for Calculating Three-Dimensional, Turbulent Incompressible Boundary Layer Flows", DLR-FB 77-16, 1977.

[17] Consteix, J.,"Progrès Théorique et moyens de précision de la couche limite turbulente tridimensionelle", ONERA Publ. No. 157, (1974).

[18] Horton, H. P., "Entrainment in Equilibrium and Non-Equilibrium Turbulent Boundary Layers", Hawker Siddely Aviation Ltd., Hatfield, Rep. No. Research/1094/HPH, 1969.

[19] van den Berg, B., and A. Elsenaar, "Measurements in a Three-Dimensional Incompressible Turbulent Boundary Layer in an Adverse Pressure Gradient under Infinite Swept Wing Conditions", NLR TR 72092 U, 1972.

[20] Stock, H. W., "Integral Procedure for Calculating Three-Dimensional, Laminar and Turbulent Boundary Layer Flows", Dornier Report 77/51B, 1977. /37

[21] Myring, D. F., "An Integral Prediction Method for Three-Dimensional Turbulent Boundary Layers in Incompressible Flow", RAE TR 70147, 1970.

[22] Hall, M. G., and H. B. Dickens, "Measurement in a Three-Dimensional Turbulent Boundary Layer in Supersonic Flow", RAE Technical Report No. 66214.

[23] Smith, P. D., "An Integral Prediction Method for Three-Dimensional Compressible Turbulent Boundary Layers", ARC, R&M No. 3739, 1974.

[24] Humphreys, D. A., "Comparison of Boundary Layer Calculations for a Wing", The May 1978 Stockholm Workshop test case, FFA TN AE-1522, 1978.

[25] Fritz, W., S. Leicher, W. Schmidt, H. W. Stock, "Continuation of the Studies for Designing Supercritical Wings for Commercial Aircraft, Part II: Theoretical Work", BMFT-FB W79-07, 1979.

[26] Stock, H. W., and H. P. Horton, "An Integral Procedure for Calculating Three-Dimensional, Laminar, Compressible, Adiabatic Boundary Layers", Do 79/77B, 1979. /38

[27] Stock, H. W., "Laminar Boundary Layers on Inclined Ellipsoids", Dornier AV No. BF30-1511/79, 1979.

[28] Geissler, W., "Calculation of the Laminar, Three-Dimensional Boundary Layer on Unsymmetrical Rotational Objects Subjected to Circulation, by means of Different Procedures", DFVLR-FB-251-73 A 19, 1973.

[29] Meier, H. U. and H. P. Kreplin, "Experimental Investigation of the Transition and Separation Phenomena on a Body of Revolution", DEA Meeting on Boundary Layer Effects, 1979.

[30] Geissler, W., "Calculation of the Laminar Separation with Unsymmetrical Rotational Objects Subject to Circulation, by means of Different Procedures", DFVLR-IB 251-73 A31, 1973.